Research Paper

Off-design of a CO₂-based mixture transcritical cycle for CSP applications: Analysis at part load and variable ambient temperature

Ettore Morosini [a,*], Dario Alfani [a], Salma I. Salah [b,e], Abdelrahman Abdeldayem [b], Francesco Crespi [c], Gioele Di Marcoberardino [d], Giampaolo Manzolini [a]

[a] Politecnico di Milano, Dipartimento di Energia, Via Lambruschini 4, Milano 20156, Italy
[b] Energy, Sustainability and Net Zero Research Centre, Department of Engineering, City, University of London, Northampton Square, London EC1V 0HB, United Kingdom
[c] Department of Energy Engineering, University of Seville, Camino de los descubrimientos s/n, Seville 41092, Spain
[d] Università degli Studi di Brescia, Dipartimento di Ingegneria Meccanica ed Industriale, via Branze, 38, 25123 Brescia, Italy
[e] Department of Mechanical Engineering, The British University in Egypt (BUE), El Sherouk City, Cairo, 11837, Egypt

A B S T R A C T

This work focuses on the off-design analysis of a simple recuperative transcritical power cycle working with the CO₂ + C₆F₆ mixture as working fluid. The cycle is air-cooled and proposed for a state-of-the-art concentrated solar plant with solar salts as heat transfer fluid in a hot region, with a cycle minimum and maximum temperature of 51 °C and 550 °C at design conditions. The design of each cycle heat exchanger (primary, recuperator and condenser) is carried out in MATLAB with referenced models and the turbine designed in CFD, providing performance maps adopted by the cycle operating in sliding pressure. The off-design of the cycle is developed with a routine simulating the thermodynamic conditions of the cycle at variable ambient temperature and thermal inputs down to 40 % of the nominal value. The results show that the cycle can efficiently run in a wide range of part load conditions and ambient temperatures, from around 0 °C to over 40 °C, with net electric cycle efficiencies from 45 % to 36 %: according to the control philosophy proposed, the condenser fans are fixed at design speed, while the cycle operates in sliding pressure, when is possible. The results evidence the flexibility and good performances of the proposed system in various operating conditions.

1. Introduction

Concentrated solar power (CSP) is widely recognized as a suitable technology to provide clean and dispatchable electric power to the grid. The adoption of a thermal energy storage (TES), decoupling electricity production from the solar radiation, is the peculiarity of CSP with respect to other more diffused, cheaper and inherently not dispatchable technologies such as PV or wind turbines. The CSP configuration with a central solar tower and a surrounded heliostat field is mostly adopted in the last years for state-of-the-art large-scale applications (above 50 MW_el).

The current state-of-the-art CSP plants integrate steam Rankine cycles as power block to the solar plant but, given the typical locations of CSP plants (normally placed in hot and arid climates), net electric power block efficiencies can be expected around 39.2 % for an ambient temperature of 30 °C [1], strongly penalized by the air condenser auxiliary consumption [2]. Moreover, the efficiency further reduces by 1.5 % when the ambient temperature moves from 30 °C to 40 °C. Finally, fast transients (both for rump-up and rump-down) and start-ups are not favored in steam cycles: a fast regulation of the load might affect the

overall competitiveness of the solar system itself, especially when competing with electric batteries.

Numerous literature studies about this technology underlined the necessity for CSP to effectively be tuned to the residual electric load: for example, a literature work [3] proposed an analysis of a large-scale steam Rankine cycle off-design control strategies under different boundary conditions when applied to a CSP plant located in California. In a follow-up work it was also evidenced that revenues are maximized when start-ups of both the solar plant and the power cycle are minimized along the year [4]. Moreover, the economic impact of a startup of a conventional Rankine was identified for a 150 MW_el solarized cycle at around 10 thousand dollars [5], with a minimum start-up time of 30 min. The authors underlined that, at constant solar plant characteristics and power block size, a cycle operation that allows for part load conditions (even below 50 % of the thermal input at design) would inevitably and drastically cut the yearly cycle start-ups and shut-downs. Other studies focused on the integration of CSP with photovoltaics (PV) to cost-effectively increase the dispatchability of the plants (running the CSP section mostly to balance the intermittency of PV): in a literature work about the comparison between PV with battery storage and PV + CSP [6], the authors highlighted that PV + CSP can be a suitable solution

---

* Corresponding author.
  E-mail address: ettore.morosini@polimi.it (E. Morosini).

Nomenclature

Acronyms

CFD	Computational Fluid Dynamics
CSP	Concentrated Solar Power
EoS	Equation of State
HTC	Heat transfer coefficient of the heat exchanger [W/m^2/K]
HTF	Heat Transfer Fluid
HX	Heat Exchanger
LCOE	Levelized Cost of Electricity [$/MWh$_{el}$]
MED	Multi Effect Distillation plant for seawater desalination
NFPA	National Fire Protection Association
PC-SAFT	Perturbed Chain Statistical Associating Fluid Theory Equation of State
PCHE	Printed Circuit Heat Exchanger
PHE	Primary Heat Exchanger
PV	Photovoltaic
sCO$_2$	Supercritical Carbon Dioxide
S&T	Shell and Tubes Heat Exchanger
TES	Thermal Energy Storage
TIT	Turbine Inlet temperature
VLE	Vapor Liquid Equilibrium of a mixture

Symbols

A	Heat Exchange Area of the Heat Exchanger [m^2]
$\dot{m}_{HTF}$	Mass flow rate of the HTF [kg/s]
$\dot{m}_{Work\ Fluid}$	Mass flow rate of the working fluid [kg/s]
$\dot{m}_{Rid}$	Reduced mass flow rate at turbine inlet
$\dot{W}_{Pump,mech}$	Mechanical power absorbed by the pump of the cycle [MW]
$\dot{W}_{Turbine,mech}$	Mechanical power produced by the turbine of the cycle [MW]
$\dot{W}_{El\ Mech,\ Losses}$	Electro-mechanical losses of the turbine and pump [MW]
$\dot{W}_{Condenser,\ AUX}$	Electric power consumed by the air-cooled condenser [MW$_{el}$]
η_{Gross}	Cycle mechanical efficiency (including the mechanical power of the turbomachinery)
$\eta_{Net\ Electric}$	Cycle electric efficiency (including electromechanical losses and the condenser consumption)
$\eta_{el,mech}$	Electromechanical efficiency of the turbine and the pump
P	Pressure [bar]
ΔP	Pressure drop [bar]
T	Temperature [°C]
ΔT	Temperature difference [°C]
ΔT_{lm}	Mean logarithmic temperature difference of the HX [°C]
$\Delta T_{Cycle-Ambient}$	Cold-end temperature difference of the condenser [°C]
$\dot{Q}_{PHE}$	Thermal power of the primary heat exchanger [MW$_{th}$]
$\dot{Q}_{Recuperator}$	Thermal power of the recuperator [MW$_{th}$]
$\dot{Q}_{COND}$	Thermal power of the condenser [MW$_{th}$]
$w_{specific}$	Specific Work of the power cycle [kJ/kg]
$\dot{V}_{air}$	Air volumetric flow rate delivered by the air-cooled condenser [m^3/s]
$\frac{V}{L}$	Ratio between the volume occupied by the vapor and the liquid phase of working fluid in the hotwell
U	Overall Heat Transfer Coefficient of a Heat Exchanger [W/m^2/K]
UA	Product between U and A of a Heat Exchanger [W/K]

---

in case 70 % of the annual load request must be satisfied.

In addition to steam cycles for CSP applications, many studies highlighted the performances of supercritical CO$_2$ power cycles (sCO$_2$) due to their cost effectiveness [7], faster transients, large operational flexibility (even when air cooling is considered [8]), a widely simplified plant layout (where no bleedings, steam drums nor deaerators are included) and a consequently reduced footprint. White summarized the main control strategies reported in literature for the simple recuperated and recompression cycles [9]. In this regard, working fluid inventory control is widely accepted as the main load control method since it achieves the highest cycle efficiency at reduced loads. The working fluid is bled from the high-pressure section of the system and stored in an inventory tank, where it can be reinjected back to the low-pressure side of the cycle when higher loads are demanded. A comprehensive steady-state and transient analysis of inventory control systems referring to a 50 kW sCO$_2$ test facility has been recently presented by Marchionni [10]. Moisseytsev [11] proposed a control strategy for a recompression CO$_2$ cycles for 100 % to 0 % the electric load, operating by (i) bypassing the turbine for load between 90 and 100 % of the nominal value, (ii) controlling the inventory as an effective operating strategy between 90 % and 50 % and (iii) turbine throttling for part-load operation from below 50 %. Furthermore, several studies focused on the operation of sCO$_2$ power systems for CSP applications: Yang [12] studied the off-design performance of a 50 MW$_{el}$ simple recuperated cycle integrated with a CSP plant. The authors fixed the turbine inlet temperature (TIT), compressor inlet temperature and compressor inlet pressure to the design values, concluding that the HTF outlet temperature varies at part-load, affecting the receiver thermal efficiency. Alfani studied the operation of a CSP plant using sodium as heat transfer fluid (HTF) and a recompression sCO$_2$ cycle under different inventory control schemes [13]. It was observed that a reduction in the compressor inlet pressure in

off-design benefits the system efficiency if compared to operating at constant inlet pressure, and that fixing the TIT produces a rise in the HTF cold temperature which may be detrimental for TES performance, due to a progressive temperature increase of the cold storage tank. The authors also modified the cycle minimum pressure to fix the HTF temperature range, resulting in a strong penalization in cycle efficiency at low thermal load. Further studies by Neises presented the off-design of a 50 MW$_{el}$ recompression sCO$_2$ cycle under the hypothesis of constant HTF outlet temperature [14]. This approach, compared to the control strategy of the previous studies (at constant TIT), reduces several thermo-mechanical problems due to the fluctuation of temperatures in the receiver and TES. More importantly, fixing the HTF temperature range avoids a reduction of the effective capacity of the TES due to an increment in the cold tank temperature. It was additionally concluded that at ambient temperatures higher than the design value it is not possible to target the HTF outlet temperature without a drop in net power output, by increasing the cycle maximum pressure.

sCO$_2$ cycles are penalized both at very low and very high ambient temperatures when air-cooled: for low temperatures the working fluid cannot approach 31 °C, the critical point of CO$_2$, due to issues in the operation of the compressor, while at high temperatures, above 50 °C of cycle minimum temperature, the real-gas effects of the pure CO$_2$ are attenuated, and the cycle efficiency is badly affected [15,16]. To improve the conversion efficiency of sCO$_2$ cycles, particularly for CSP applications, different working fluids, such as CO$_2$-based mixtures, are proposed to fit the operating conditions of the working fluid with the high ambient temperature of the location [17]. The addition of a dopant to CO$_2$ increases the critical temperature of the mixture, allowing to compress the working fluid in liquid phase with a pump, instead of in supercritical phase, further reducing the compression work. This concept is investigated within two H2020 EU projects, SCARABEUS [18]

and DESOLINATION [19], with the aim of proving from a thermodynamic point of view power conversion efficiencies over 50 % with cycles minimum temperatures above 50 °C.

Between the CO_2 dopants investigated within the SCARABEUS projects, as SO_2 [20,21] and $TiCl_4$ [22,23], this work focuses on the use of C_6F_6 (hexafluorobenzene) due to its higher compatibility and easier management, to exploit a safe and inert compound which can be more attractive from an industrial perspective. C_6F_6, has a good thermal stability, very low toxicity levels a high boiling temperature at ambient pressure (around 81 °C) and a low flammability. Experimental VLE data have been taken on the $CO_2 + C_6F_6$ mixture, along with the analysis of the mixture thermal stability [24], that has proven the suitability of the mixture to be adopted as working fluid for cycles maximum temperatures up to 600 °C, testing the fluid decomposition in an Inconel 625 vessel for 100 h. Finally, the fluid is inert when put in contact with other substances, such as air, water or CO_2. According to the NFPA 704 classification, the substance has a health index of 2, a flammability index of 1 (as the flash point of the fluid is 10 °C) and a reactiveness index of 0.

Regarding the performance of the innovative power block with the $CO_2 + C_6F_6$ mixture as working fluid, various studies in literature underlined its good characteristics and nominal performances, especially for CSP applications: in the works of Manzolini [25] and Morosini [26] a complete techno-economic analysis the solar plant was carried out, including the solar subsystems such as receiver and solar field, for large scale applications. Other works focused on the coupling between this power cycle and a thermal desalination plant adopting multi effect distillation (MED) [27], and an analysis of a small-scale linear Fresnel CSP plant located in Sicily was also proposed studied [28]. Despite the annual assessments of the CSP plant carried out in these literature works, computing the annual energy produced and the corresponding LCOE, the dependency on the ambient temperature of the cycle conditions was not investigated. In previous literature works, the cycle conditions were considered fixed along the whole year, at constant minimum cycle pressure and temperature, with a little penalization of cycle efficiencies when the ambient temperature approaches the cycle minimum temperature due to an increment of the electric consumption of the air-cooled condenser fans [29]. In addition, no part load operations were carried out nor investigated, aiming at running the cycle always at full load to maximize its efficiency. This work aims at closing this gap, considering crucial both describing the off-design performances of the solar plant along the year and modelling the cycle in part load operations. To achieve this objective, accurate numerical models of each cycle component have been developed adopting tailored correlations for the estimation of the CO_2-based mixture heat transfer coefficients and the pressure drops. The off-design operation of the air-cooled CO_2-based power cycle is described by means of performance maps for a wide range of thermal input and ambient temperature, ideally providing a methodology to assess the cycle performance for any CO_2-based working fluid.

2. Scope of the work and cycle conditions at design

The aim of this work is to model the off-design behavior of a simple recuperative power cycle working with the $CO_2 + C_6F_6$ mixture as working fluid, assuming a state-of-the-art CSP plant with central receiver and solar salts as HTF [30]. Other studies in literature presented analyses with pure CO_2 as working fluid in supercritical cycles but, according to the knowledge of the authors, this is the first work which provides a detailed off-design analysis of a power cycle with CO_2-based mixtures as working fluid for CSP applications. The simple recuperative configuration is adopted because of its simplicity, good performance and higher flexibility with respect to more complex layouts that can include two compression steps, splitters of the mass flow rate or multiple turbines and regenerators [31,32].

The mixture thermodynamic properties are computed with Aspen Plus v.11 [33] adopting the PC-SAFT EoS [34], which is based on the proper fitting on the pure component behavior [35] with a temperature-dependent binary interaction parameter [24]. The working fluid composition is selected at 87 % CO_2 molar content, since it represents the condition at maximum cycle efficiency for the selected power block layout [35]. Future works can also develop analysis at variable mixture compositions, as literature works evidenced the possible advantages in terms of cycle efficiency [36]. The transport properties are computed according to a literature work on this specific mixture [37], with models calibrated on the behavior of the pure components (both CO_2 and C_6F_6).

The cycle is designed to produce 100 MW at nominal power. The main assumptions related to the cycle design conditions are reported in Table 1, and the power block layout is proposed in Fig. 1. The schematic consists of a variable speed pump driven by an electric motor, a recuperator that cools down the flow at the outlet of the turbine, a primary heat exchanger where the working fluid is heated up to the cycle maximum temperature by cooling down the HTF, an axial turbine with a direct-drive generator and an air-cooled condenser that release heat to the environment cooling down and condensing the working fluid to the minimum cycle temperature. Regarding the air-cooled condenser, the design is carried out at an ambient temperature of 36 °C (a value that is strongly location-dependent), considering a cycle minimum temperature of 51 °C. A hotwell is placed between the pump and the condenser to accommodate the working fluid at the condenser outlet and define the thermodynamic conditions of the pumped fluid: this component is not preset in sCO_2 cycles, but it is necessary to separate the two phases of the transcritical cycle after the condensation. The power block layout is completed by a variable-volume working fluid storage vessel, containing the $CO_2 + C_6F_6$ mixture at nominal composition in liquid phase, at an intermediate pressure between the cycle maximum and minimum pressure.

Fig. 2 depicts the power cycle in the main thermodynamic diagrams: the critical point of the working fluid is a condition very close to the cricondenbar, of around 100 °C and 135 bar. The cycle thermodynamic conditions are also reported in Table 2, and a complete table of the

Table 1
Assumption on the cycle characteristics at design conditions.

| Variable	Value at design conditions	Notes
Cycle minimum temperature [°C]	51	For air-cooled heat rejection in hot environments
Cycle maximum temperature [°C]	550	According to state-of-the-art CSP
Turbine inlet pressure [bar]	252	Computed to meet ΔP requirements
Pump inlet pressure [bar]	84.5	At bubble conditions
Recuperator minimum internal temperature difference [°C]	5	According to literature [25]
Turbine isentropic efficiency [%]	92.1	According to the turbine maps of this work
Pump isentropic efficiency [%]	88	According to industrial partner of SCARABEUS
Primary HX pressure drops [bar]	2	According to literature [26]
Condenser pressure drops [bar]	1	Assumed in the MATLAB model of this work
PCHE pressure drops (low pressure) [bar]	1	Assumed in the MATLAB model of this work
PCHE pressure drops (high pressure) [bar]	0.35	Computed by the recuperator MATLAB model
Motor and generator electromechanical efficiency [%]	99	According to literature [26]
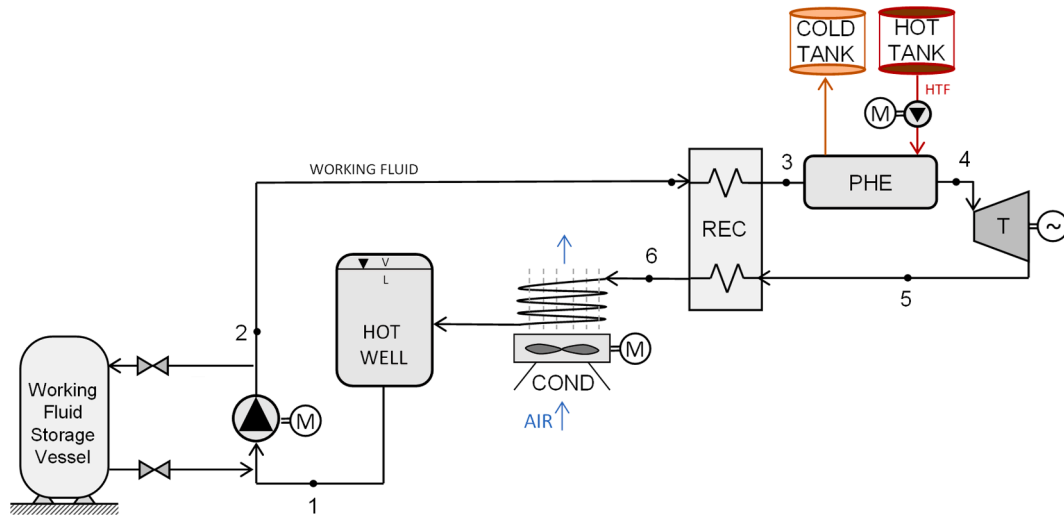
Fig. 1. Plant layout of the transcritical cycle working with the $CO_2 + C_6F_6$ mixture.
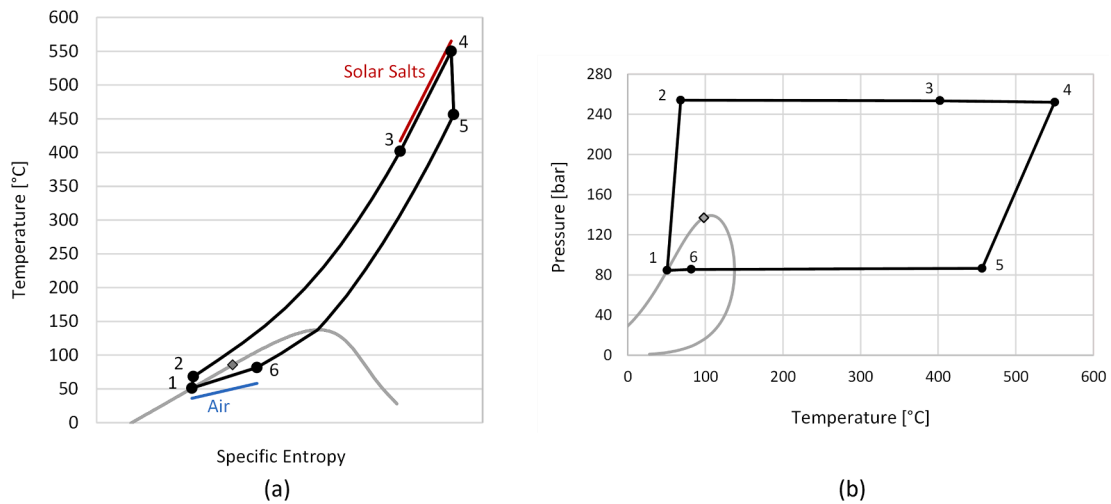

Fig. 2. Power cycle at design conditions in the T-s diagram (a) and the P-T diagram (b).

Table 2
Thermodynamic conditions of the transcritical $CO_2 + C_6F_6$ cycle at design.

Thermodynamic condition	1	2	3	4	5	6
Temperature [°C]	51.0	67.9	401.3	550.0	455.9	81.2
Pressure [bar]	84.5	254.3	254.0	252.0	86.5	85.5
Enthalpy [kJ/kg]	0	19.8	530.6	727.0	624.0	113.2

thermal and mechanical power balances is shown in Table 3. The molar vapor quality at condenser inlet (point 6) is equal to 69 %.

The analysis proposed in this work, depicted in the flowchart of in Fig. 3, aims at assessing the off-design behavior of the cycle, regardless the solar plant operation. The cycle is firstly modelled at design conditions from a thermodynamic point of view, adopting the software ASPEN Plus. Then, all the power cycle components are designed using as input
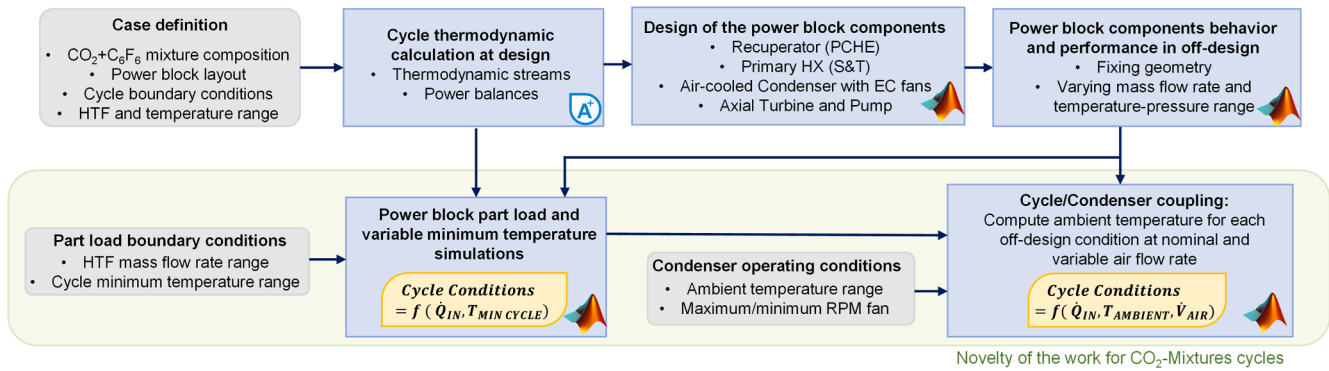
Table 3
Thermal and mechanical power balance of the cycle at design conditions.

Variable	Value at design conditions
Working fluid flow rate [kg/s]	1202.3
Gross specific work [kJ/kg]	83.2
Pump mechanical power [MW]	23.9
Turbine mechanical power [MW]	123.9
Recuperator heat duty [MW$_{th}$]	614.0
PHE heat duty [MW$_{th}$]	236.1
Condenser heat duty [MW$_{th}$]	136.1
UA$_{PCHE}$/PHE heat duty [1/K]	0.15
Gross cycle efficiency [%]	42.36
Electromechanical losses, condenser consumption [MW$_{el}$]	2.2
Net electric cycle efficiency [%]	41.42

Fig. 3. Overview of the analysis proposed in this work.

the results of the thermodynamic simulation: the heat exchangers are designed with validated 1-D MATLAB codes and the axial turbine is designed through CFD analysis. The thermodynamic variables and the transport properties of the mixture are provided to the MATLAB routines in forms of a series of isobaric lookup tables, with a fine resolution both in temperature and pressure.

The design and preliminary sizing of the cycle components is necessary to simulate their behavior in off-design operation, due to variations of both the ambient temperature and thermal input.

The off-design analysis of the cycle is divided into two subsequent steps. At first, the cycle is simulated for various levels of thermal input and cycle minimum temperature, not considering the off-design operation of the air-cooled condenser. Then, a second analysis is carried out considering the cycle off-design solutions as input: this second set of simulations computes only the off-design of the condenser (knowing the mass flow rate, the temperature and pressure range of the working fluid across the condenser at any condition), over a wide range of ambient temperatures. As a result, for each off-design condition and each ambient temperature, the model can compute the velocity of the air (hence the mass flow rate of air across the air-condenser and its electrical consumption) necessary to solve the condenser model.

In the next chapters the work will be developed as follows: Chapter 3 underlines the methodology adopted while computing the off-design of the cycle. Since the analysis of the cycle off-design must foresee a detailed sizing of the cycle components, their design criteria are also highlighted. Chapter 4 shows the actual sizing of the power plant with the innovative working fluid and Chapter 5 evidence the resulting off-design performances of the plant, focusing on the interaction between the power cycle and the air-cooled condenser.

3. Methodology

3.1. Cycle off-design and part load analysis: Boundary conditions

Only steady-state conditions are considered in this work, as dynamic simulations are beyond the scope of this work since they require different numerical tools accounting for the thermal and mechanical inertias of the components. The independent variables of the analysis are listed in Table 4, while the control options, with the corresponding control variables, are listed in Table 5: the thermal input to the power cycle is regulated through the mass flow rate of the HTF by varying the HTF pump rotational speed, the heat rejection from the power cycle is

Table 4
Indipendent variables of the analysis of the cycle in off-design.

Independent Variables
HTF pump rotational speed (HTF mass flow rate)
Ambient temperature

Table 5
Controlled options and controlled variables of the power plant while operating in off-design.

Controlled Options	Controlled Variables
Rotational speed of the condenser fans (Air mass flow rate)	Working fluid conditions at pump inlet
Conditions of the working fluid storage vessel	Hotwell level
Rotational speed of the cycle pump	Working fluid mass flow rate

Table 6
Boundary conditions of the power block operating in off-design.

Off-design Boundary Conditions
$140\,bar < P_{in,turb} < 252\,bar$
$58\,bar < P_{min} < 84\,bar$
$31°C < T_{min,cycle} < 51°C$
$TIT < 561°C$
$T_{hot,tank} = 565°C$
$T_{out,HTF} = 420°C$ if $\left(T_{out,HTF} - T_3\right) > 4°C$
$\left(T_{out,HTF} - T_3\right) = 4°C$ if $T_3 > 416°C$
$30\% \cdot \dot{V}_{air,design} \leq \dot{V}_{air} \leq 130\% \cdot \dot{V}_{air,design}$
Hotwell Negligible Vapor Fraction $\left(\frac{V}{L} \to 0\right)$

regulated through the cooling air mass flow rate, varied by means of the electronically commutated (EC) axial fans. Any variation of the inventory of the power cycle is compensated through careful management of the working fluid storage vessel, that can introduce or remove working fluid from the working fluid loop. Finally, the mass flow rate of the working fluid itself is regulated with the variation of the rotational speed of the pump.

Some important boundary conditions are listed in Table 6 and are imposed to limit the solutions reached by the off-design numerical solver. The cycle maximum pressure must be always lower than its nominal value due to the mechanical limits of the materials and higher than the cricondenbar of the mixture, in order to avoid VLE conditions in the high-pressure side of the PCHE and to limit the size of the inventory of the working fluid (as large inventory vessels would be necessary to reach very low cycle minimum pressures). Since the cycle minimum pressure and temperature are univocally determined by the phase behavior of the mixture at bubble conditions, differently than sCO$_2$ cycles, cycle minimum temperatures above design value are not considered, as that would lead to a maximum pressure above the mentioned limiting upper bound.

The temperature of the hot tank of the TES is fixed at 565 °C, equal to the HTF temperature at solar receiver outlet and representing the maximum temperature of the hot source of the power cycle. Given the

non-perfect counter-current arrangement of the S&T HX, the minimum temperature difference (pinch) both at the hot-end and the cold-end of the PHE is fixed at 4 °C: accordingly, this introduces limits on the maximum temperature of the cycle (TIT) and the maximum working fluid temperature at PHE inlet (T_3). If the limit on the cold-end minimum pinch cannot be satisfied, at very low thermal load into the power cycle, the model includes the possibility to increase the outlet temperature of the HTF across the PHE: nevertheless, if this condition occurs for a large fraction of the yearly operating hours it may indicate an inappropriate design of the PHE, as this would lead to an increment of the cold tank temperature, varying the operating conditions of the receiver and badly affecting its thermal efficiency and the pressure drops of the HTF.

Regarding the flexibility of the heat rejection unit, the EC fans of the air-condenser are supposed to deliver a variable air volumetric flow rate, from a minimum of 30 % to a maximum of 130 % of the design value.

Finally, the working fluid storage vessel is regulated always to have a negligible vapor fraction in the hotwell. This last condition is crucial while handling mixtures as working fluids for transcritical cycles. While in power cycles working with pure fluids (e.g., steam Rankine cycles) the hotwell can experience a variable free surface level during off-design conditions, this cannot be a viable solution when mixtures are adopted as working fluids, as the vapor and liquid phases compositions in the hotwell are different. For this reason, a variation of the hotwell free surface level would inevitably cause a change of the liquid phase composition, that, circulated by the pump, would cause a variation of the working fluid composition in the power cycle.

3.2. Cycle off-design and part load analysis: Methodology

The overall outlook of the methodology adopted to solve the cycle in off-design conditions is illustrated in Fig. 4. The off-design simulations require the definition of both the thermal input to the power cycle (defined through the mass flow rate of HTF) and the cycle minimum pressure and temperature. Then, the iterative procedure starts guessing a value of the cycle maximum temperature (T_4), the pressure at turbine inlet (P_4), the working fluid temperature at PHE inlet (T_3) and the cycle mass flow rate. Running the code of the PHE in off-design, the procedure updates each of these four variables according to the methodology proposed in the figure considering the operation of the cycle in sliding pressure.

When the off-design sub-routine of the PHE is solved, the turbine and pump isentropic efficiencies are estimated from the respective turbomachinery maps, and the turbine outlet temperature (T_5) and pump outlet temperature (T_2) are directly computed. Finally, the recuperator model is run in off-design conditions to reach convergence on the temperature at PHE inlet (T_3). If the recuperator off-design model does not provide the same results on T_3 than the value initially assumed, T_3 is updated, and the overall process is iteratively reproposed up to convergence on T_3. Once the convergence on T_3 is reached, the cycle is univocally solved. A comparison between the MATLAB solution and the calculation of ASPEN Plus is carried out in the end, to verify convergency on the last variable T_6. The iterative procedure is then repeated for different input values of HTF mass flow rate and cycle minimum temperature and pressure.
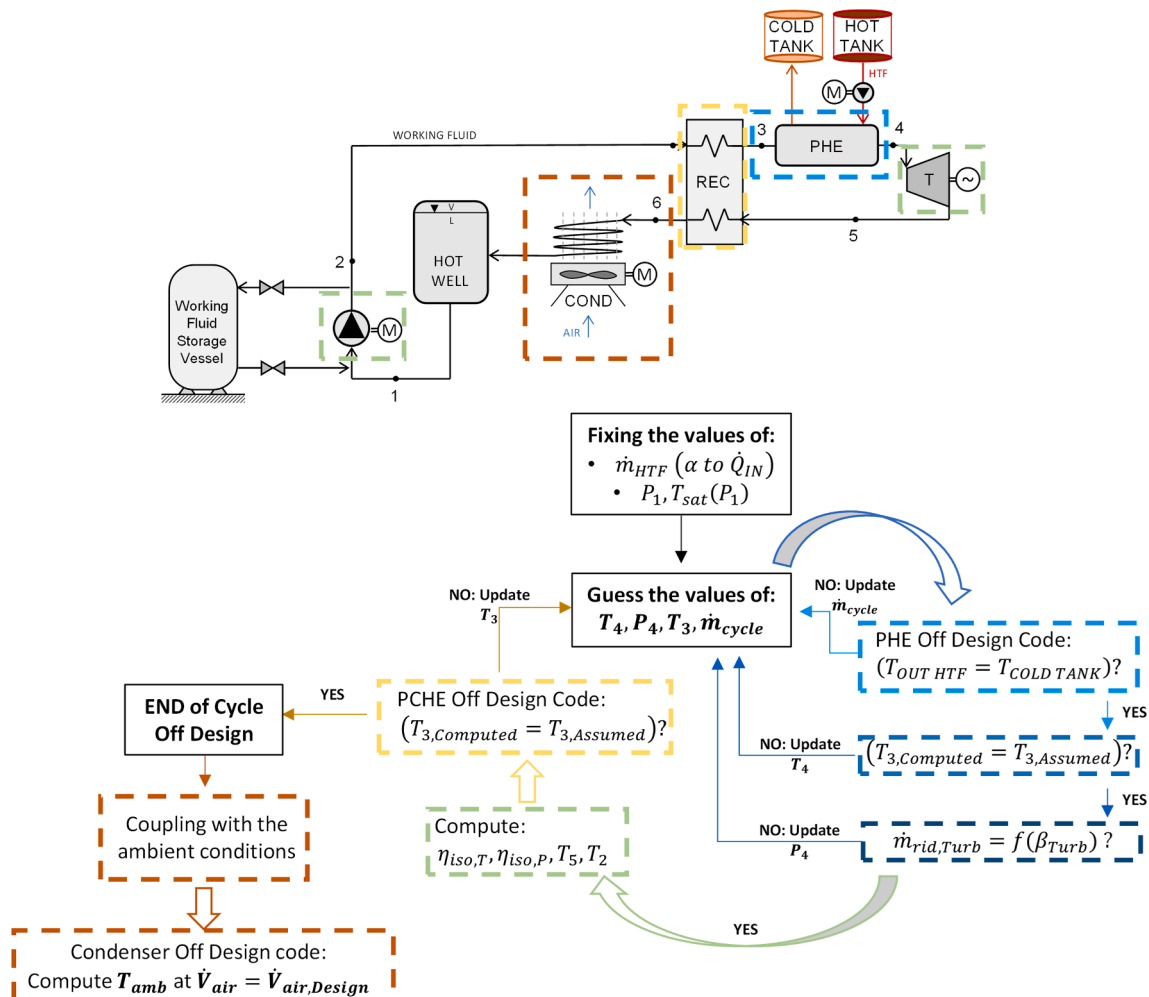

Fig. 4. Methodology adopted for the analysis of the power block in off-design conditions.

As the independent variables of the system are the HTF mass flow rate and the ambient temperature, a specific ambient temperature is associated with each cycle solution through the off-design model of the air-condenser at constant fan speed, fixed at design value. In fact, in off-design, the proposed control philosophy of the air-cooled condenser is to run the fans at design rotational speed, without any penalization on the fan hydraulic efficiency, always delivering the same air volumetric flow rate.

Once all cycle off-design simulations are associated with an ambient temperature at constant air flow rate, the ambient temperature range is extended by assuming other values of fan rotational speed, down to 30 % of the nominal value and up to 130 % of the nominal value. In these cases, a new value of ambient temperature is computed at different air face velocities with the off-design code of the condenser, keeping constant the solutions of the cycle reached in sliding pressure conditions on the working fluid side (flow rate, temperature and pressure at both inlet and outlet of the condenser). Additional details on the off-design simulations numerical modes are provided in Appendix D.

3.3. Cycle components modeling

The heat exchangers of the power cycle are fully designed with 1D finite volume MATLAB models, while the axial turbine is designed through a CFD analysis carried out with commercial software. Only the characteristics of the pump, provided by an industrial partner of the SCARABEUS project, are not detailed in this chapter due to an NDA with the manufacturer.

3.3.1. Turbine

The turbine design process is initiated using mean-line in-house design tool (1D) to create the flow path design and form the base for the 3D numerical simulations, presented by the authors in previous literature works [38–40]. The preliminary flow path design aims at achieving the highest aerodynamic performance alongside complying with a set of mechanical and rotodynamic considerations. The mechanical and aerodynamic design constraints are set based on industrial experience to allow for providing feasible machine designs from a practical standpoint, such as the blades stress limits and the flow path slenderness ratio, the ratio of bearing span with respect to the hub diameter. Loading coefficient, flow coefficient, degree of reaction and pitch-to-chord ratio of 1.0, 0.5, 0.5 and 0.85, respectively, are assumed constant within the mean line design. Those parameters are selected based on literature recommendations to achieve a high aerodynamic performance [41,42].

According to the earlier analysis conducted by the authors [40,43], reducing the hub diameter was found to result in a better turbine performance and in a longer flow path associated with a larger number of stages. On this matter, the number of design stages and rotor blades are selected to allow for a higher aerodynamic performance alongside complying to the mechanical and rotodynamic design criteria. To ensure the mechanical integrity of the blades, the static bending stress limit is set to 130 MPa and a slenderness ratio lower than 9 [39]. Therefore, nine design stages are selected to optimize the aerodynamic performance of the C_6F_6 flow path and the number of blades range between 35 and 95 across the stages to comply with the mechanical design criteria. With the known number of stages and defined parameters, the thermodynamic properties at the stator and rotor alongside the velocity triangles are all obtained for the flow path. Hence, the detailed blade geometry is obtained, including blade heights, annulus area, chord and axial chord length, blade pitch, and throat-to-pitch ratio (o/c). The turbine performance is evaluated in the 1D mean-line methodology using the Aungier loss model correlations where profile, secondary flow, tip clearance, trailing edge losses are all included [44]. Given that the machine is designed to operate for a 100 MW plant, a synchronous machine is selected due to the difficulty of incorporating a gearbox for such turbine scales, making non-synchronous generator designs hard to implement.

Following the 1D flow path design, the 3D blades are generated assuming several geometric parameters to fully define the 3D blade shape such as leading-edge thickness, inlet/outlet wedge angles, airfoil curvature control points, and blade base fillet. These assumptions are made based on a previous blade shape optimization study conducted by the some of the authors [45]. The 2D aerofoil is then extruded to form the 3D blade since the mean-line design indicates relatively short blades compared to the blade's mean diameter. As a part of the CFD simulations, the predicted mass flow rate is compared to the mass flow dictated by the cycle analysis and consequently the 3D blade design assumptions are adjusted to provide a better match with the cycle parameters. The CFD analysis is carried out using ANSYS workbench where ANYSY-CFX solver, bladeGen and TurboGrid are used to simulate the flow and generate the blade profile and the mesh respectively. Within the conducted CFD analysis, a steady-state multi-stage CFD model is set up for a single flow passage, where a mixing plane interface is defined between the stator and rotor blades. In the developed design, total pressure and total temperature are used to model the stator inlet conditions whereas the static pressure is defined at the turbine outlet.

3.3.2. Recuperator

The recuperator of the power cycle investigated is designed as a Printed Circuit Heat Exchanger (PCHE) with standard straight semi-circular channels, in accordance with the work of Dostal [46].

Appendix E contains all the design parameters employed to compute the PCHE design, assumed considering literature values for all the geometrical parameters among the sCO_2 cycles field [47]. With respect to literature works on sCO_2 power cycles, in this work the model is extended to characterize condensing flows in the low-pressure side of the recuperator, introducing two-phases fluid flow correlations of heat transfer coefficients (HTC) and pressure drops.

The convective heat transfer coefficient of the single-phase fluid is computed with the Gnielinski correlation [48], while for two-phase condensing flows the Cavallini model is employed [49], as already proposed in literature for this working fluid mixture [37]. The in-channel pressure drops are computed with the Darcy–Weisbach equation, adopting the Chen correlation for the friction factor [26] (as it has the accuracy of the Colebrook-White correlation, but it is explicit in the friction factor), while the pressure drops in the VLE region are computed with the Del Col model for azeotropic mixtures [50], as proposed in literature for condensing CO_2-mixtures [26].

The design of the PCHE is carried out with a given mass velocity for each channel, simulated with a discretization of 300 finite volumes. For every finite volume, the energy balance equation and the heat exchanger constitutive equation are solved simultaneously, and the overall heat transfer coefficient is computed. By means of a numerical solver, the code iterates on the in-channel mass velocity until it converges to the desired pressure drops. The main outputs of the code are the channels length, the overall number of channels and the axial profile of the main thermodynamic and heat transfer variables, such as the heat transfer coefficients, the velocities, the densities and the pressure drop. Additional descriptions on the PCHE MATLAB model can be found in Appendix A.

3.3.3. Primary HX

The primary HX of the power cycle considered in this work is a single-pass shell-and-tube HX, modelled and sized in MATLAB adopting the Bell and Delaware methodology as presented by Fettaka [51], and already adopted in literature for the design of PHE for CO_2-based power cycles [26]. The model adopts the main HX geometrical characteristics among the range suggested by Kakaç [52], such as the tube arrangement angle, tube geometry, baffle spacing to shell diameter ratio, baffle cut to shell diameter ratio and tube pitch to outer diameter ratio. Due to the high temperature application, Inconel 617 is adopted as material (as stainless steel is suggested in a lower operating temperature range [53]). The tube-side heat transfer coefficient and pressure drop calculations are modelled the same way as for the recuperator when working in single
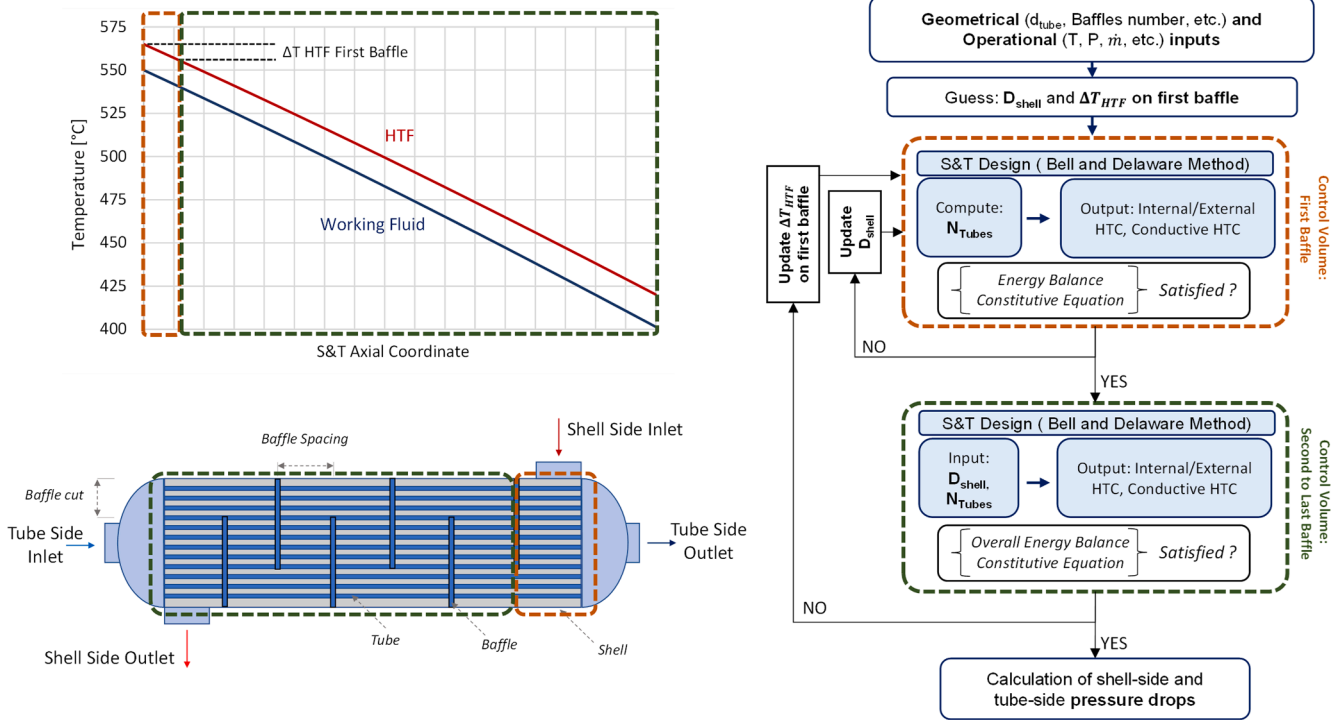
Fig. 5. Methodology for the design of the S&T PHE of the power cycle.

phase conditions, while the Bell and Delaware method is adopted for the calculation of the shell-side heat transfer coefficient and pressure drop [26,51]. The method is developed with a finite-volume approach as for the recuperator, considering a single finite-volume for each region between baffles. The S&T PHE adopted in this work has the geometrical and material characteristics listed in Appendix D.

The flowchart proposed in Fig. 5 describes the iterative procedure to size the S&T PHE: initially, the number of tubes and the dimensions of the shell are assessed based on calculations on the first finite volume, then the S&T geometry is fixed and all the remaining finite volumes (from the second to the last) are solved iteratively up to convergency on the energy balance and constitutive equation of each HX baffle. Finally, the overall heat exchanger energy balance and constitutive equation are checked and, if these two conditions are not satisfied, the numerical tool updates the number of tubes and shell dimensions until it reaches the

overall convergence. As the convergence is reached, the S&T PHE sizing numerical tool checks the mechanical integrity of the tubes using the correlation proposed in literature, considering an additional safety factor of 1.15 [54]. A validation of the MATLAB model developed in this work has been carried out considering the design results of THERMO-FLEX on some case studies, and it is shown in Appendix B.

3.3.4. Air cooled condenser

The air-cooled condenser is sized by means of a numerical model developed in the framework of the SCARABEUS project and validated with an industrial partner of the project consortium [37]. In the condenser, the working fluid flows inside a series of tube bundles, arranged in 7 passes and 7 loops in a staggered configuration and disposed in an air-cooled condenser with induced draft fans. The developed MATLAB model computes the number and length of the tubes to satisfy
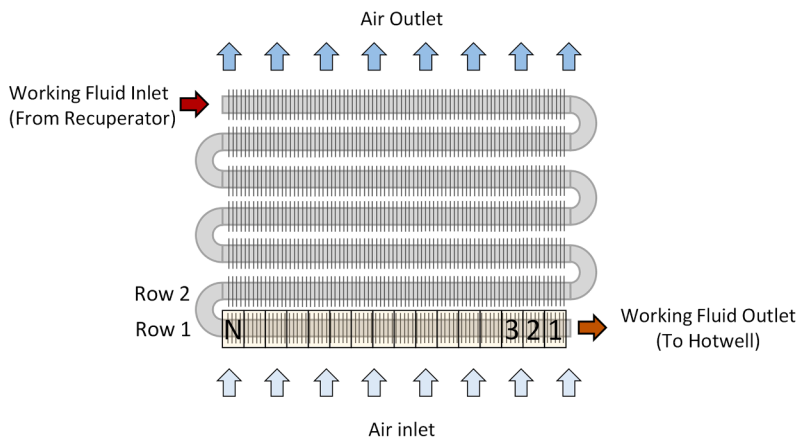

Fig. 6. Methodology for the design of the finned tubes of the air-cooled condenser of the power cycle.
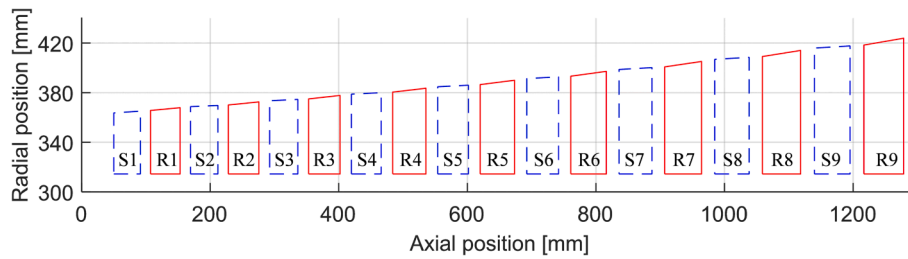
Fig. 7. Meridian view of the axial turbine designed for the power cycle.

the required heat duty and the pressure drops on the working fluid-side. The tube and fin main characteristics are defined by a SCARABEUS industrial partner [37] and are here reported in Appendix E. Fig. 6 proposes the flowchart of the overall methodology adopted by the model. Each pass of the tube is discretized in 20 finite volumes and for each of them the heat transfer problem and the pressure drops are computed iteratively, starting from the last finite volume (working fluid outlet), backwards up to the first one (the working fluid inlet). For the solution of the heat transfer problem on each finite volume, the air side heat transfer coefficient is computed according to the Grimison correlation for staggered tubes [55], while the internal one according to Cavallini, as for the PCHE.

Similarly, also for this component the tube side pressure drops are modelled with the Del Col model, while the air side pressure drops are computed with a literature correlation that has been tailored to the specific tube and fins geometry proposed by Marković [56]. The calculations are carried out in this work assuming a design value of the axial fan overall efficiency of 43 %, a value that includes the fan hydraulic efficiency and the electric efficiency of the motor.

4. Sizing of the power block components

4.1. Turbine design

As a result of the 1D modeling of the turbine, a flow path with nine stages is designed with a hub diameter of 628 mm as shown in Fig. 7. A total-to-total turbine efficiency of 92.1 % is achieved for the design conditions of the turbine reported in Table 2 and for a turbine rotational speed of 3000 rpm. In this work, the turbine total-to-total efficiency is expected to mimic the trend of the isentropic efficiency, since the adoption of an ideal diffuser at the outlet of the last stage is assumed.

The off-design performance of the defined flow path is then evaluated to investigate the turbine performance over a wide range of operating conditions. This has been achieved by varying the inlet turbine

pressure while maintaining the outlet pressure and turbine maximum temperature equal to the nominal ones. The performance map of the considered flow path is presented in Fig. 8. The map defines the pressure ratio and total-to-total turbine efficiency as function of the reduced mass flow rate, which is defined as in Equation (1), where $\dot{m}$ is the mass flow rate, R is the gas constant, T_{01} is the total turbine inlet temperature, P_{01} is the total turbine inlet pressure, D is the turbine hub diameter.

$$m_{red} = \frac{\dot{m}\sqrt{\gamma R T_{01}}}{D^2 P_{01}} \tag{1}$$

The presented range of reduced mass flow rate corresponds to a working fluid mass flow rate variation from 61 to 100 % of the design flow rate. A decrease of the reduced mass flow rate from 100 % to 93.5 % of the design value (minimum value of the map), results in a reduction in the operating total-to-total pressure ratio which passes from 2.88 to approximately 1.85. This results in a reduction in the total-to-total turbine efficiency from approximately 92.1 to 85.8 %. On the other hand, for reduced mass flow rates higher than the nominal value, it is possible to notice an almost flat trend of the turbine efficiency. As in off-design conditions the power cycle is operating in sliding pressure, there is a strong dependence between the pressure ratio and the reduced mass flow rate. Thus, there is no linear dependence between the reduced mass flow rate and the mass flow rate flowing in the cycle, due to the variation of the maximum pressure of the cycle.

By investigating the reasons behind the efficiency drop away from the design point with the CFD tool, it has been found that the flow starts to separate from the blade suction side surface due to the mismatch between the blade and flow angles at the blade inlet, which increase the aerodynamic losses and significantly decrease the blade loading at part load operating conditions. By investigating the velocity distribution obtained in CFD, it is possible to estimate that the separation starts at the last turbine stage for mass flow rate values below 81 % and this effect increases and expands to the precedent stages as the mass flow decrease. The flow structure is compared between the design point and an off-design point with 61 % mass flow rate with respect to nominal conditions, as shown in Fig. 9. In this last case, it can be seen from the figure that the flow separation is already present in the 4th turbine stage, significantly affecting the turbine performance. Additional details on the mesh adopted in this CFD case study are reported in Appendix F.

4.2. Recuperator design

The design conditions at the inlet and outlet of the recuperator of the power cycle are proposed in Table 2, while the respective T-Q diagram is shown in Fig. 10: for the considered working fluid, the minimum internal temperature difference of the countercurrent heat exchanger (5 °C, as reported in Table 1) is located where the low-pressure side fluid (recuperator hot side) starts condensing, at around 25 % of the heat exchanged, as evidenced in the T-Q diagram. The high-pressure side, on the other hand, being at a high reduced pressure (ratio between the local pressure and the critical pressure of the mixture, in this case equal to around 2), does not show large specific heat capacity variations while
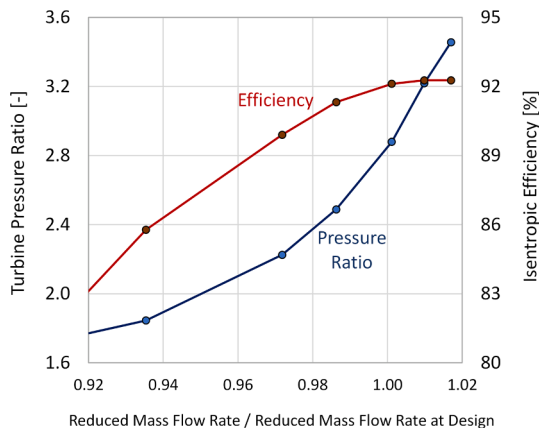

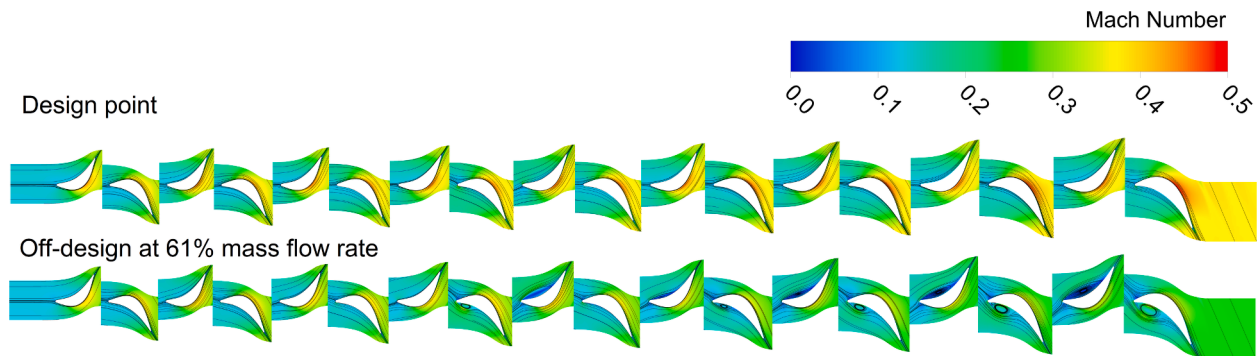**Fig. 8.** Off-design map of the turbine of the power cycle.

Fig. 9. Contour plot of Mach number of the flow across the expansion at two representative conditions (design and minimum mass flow rate investigated in the analysis).
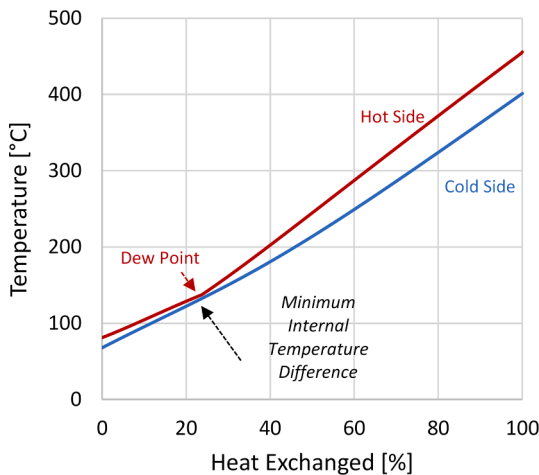

Fig. 10. Temperature-Thermal duty diagram of the recuperator of the cycle at design conditions.

Table 7
Geometrical and operational characteristics of the PCHE of the cycle.

Parameter	Value
Channel length [m]	4.42
Number of channels	1'530'430
Hot side pressure drop [bar]	1.0
Cold side pressure drop [bar]	0.3
Mass velocity [kg/s/m^2]	500
Fluid velocity, hot side [m/s]	From 2.3 to 5.5
Fluid velocity, cold side [m/s]	From 0.5 to 1.8
Average overall HTC [W/m^2/K]	1032

moving from the supercritical region to the liquid region.

The design of the PCHE recuperator is carried out to meet the required pressure drop of 1 bar on the low-pressure side features a mass velocity of 500 kg/s/m^2 and a consequent cold side pressure drop of 0.3 bar. The overall results of the PCHE model are proposed in Table 7.

A particular focus on the PCHE recuperator is dedicated to the in-channel axial distribution of the convective heat transfer coefficients (proposed in Fig. 11) and to the pressure drops per unit length on both channels (shown in Fig. 12). The convective HTC presents no discontinuities along the cold channel while, for the hot channel, a strong discontinuity (+10 %) is noticeable when the flow moves from vapor conditions (modelled with the Gnielinski correlation) to two-phase conditions (computed according to the Cavallini model). At the same time, the high-pressure and high-density working fluid on the cold side presents a velocity significantly lower than the low-pressure side, as reported in Table 7, entailing a lower pressure drop per unit length, with a linear trend along the channel. On the other hand, similar to the heat transfer coefficients, the hot-side channel experiences a discontinuity on the pressure drop per unit length, moving from the vapor region (adopting the Darcy–Weisbach equation and computing the friction factor with the Chen correlation) to the VLE (modelled with the Del Col model).

4.3. Primary HX design

The designed S&T PHE of the power cycle adopts conventional solar salts on the shell side, cooled down from 565 °C to 420 °C, at design conditions. The PHE is sized for a working fluid pressure drop of 2 bar, computing the shell size and tube number and length, varying the number of baffles. The resulting characteristics of the PHE are listed in Table 8, outlining an average value of the overall HTC of 869 W/m^2/K referred to the overall tube external area. With respect to the recuperator, where the contribution of the conductive resistance is minor (but not negligible), for the S&T PHE the relative contribution of the conduction along the tube thickness is significant.

4.4. Air cooled condenser design

The most crucial parameters for the design of the condenser are the ambient temperature and the air face velocity on the tubes. In this work, the ambient temperature in design conditions is fixed at 36 °C, representative of a hot condition in summer, and the air face velocity is fixed at a 2.6 m/s, a value that guarantees a target electric consumption of the fan around 0.8 MW$_{el}$ at design conditions (a low parasitic consumption for the power cycle, around 0.6 % of the rejected heat). The condenser sizing is carried out considering the inlet and outlet working fluid conditions reported in Table 2, aiming at a target value of the working fluid pressure drop of 1 bar. The model provides the number of tubes and their length, along with the air side pressure drop and outlet temperature. The results of the condenser design are reported in Table 9: the computed temperature difference on the air side is 23 °C, higher than typical air-cooled condensers adopted in steam cycles because of the non-isothermal heat rejection from the power cycle.

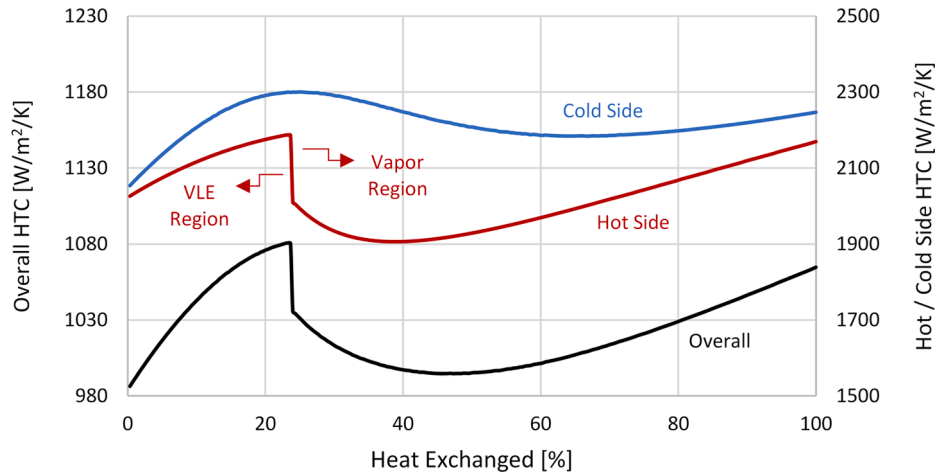Appendix C provides the results of a parametric analysis carried out

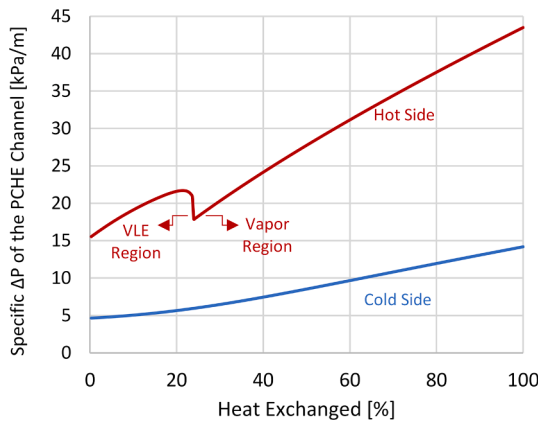**Fig. 11.** Heat transfer coefficients (convective and overall) of the PCHE along the channel.

Fig. 12. Pressure drop per unit of length of the PCHE along the channel.

Table 9

Geometrical and operational characteristics of the air-cooled condenser of the cycle.

Parameter	Value
Number of Tubes	2′795
Tube overall length/Pass length [m]	74.6/10.7
External finned condenser area (air side) [m^2]	370′924
Ambient temperature [°C]	36
Air velocity on the tube [m/s]	2.6
Air temperature difference [°C]	23.0
Air mass flow rate [kg/s]	5892
Minimum Internal Temperature Difference [°C]	12.0
Working fluid pressure drop [bar]	1
Working fluid velocity [m/s]	From 3.7 to 1.4
Working fluid mass velocity [kg/s/m^2]	1271
Air side pressure drop [Pa]	72
Overall HTC [W/m^2/K] (referring to external area)	24.9
Electric Fan Consumption [MW$_{el}$]	0.80

Table 8

Geometrical and operational characteristics of the S&T PHE of the cycle.

Parameter	Value
Tube length [m]	27.2
Number of tubes	11′514
Tubes external area [m^2]	16′740
Number of baffles	16
Shell diameter [m]	3.20
Tube side pressure drop [bar]	2.0
Shell side pressure drop [bar]	0.3
Working fluid velocity, tube side [m/s]	From 4.8 (cold end) to 6 (hot end)
Working fluid mass velocity [kg/s/m^2]	1392
Shell side convective HTC [W/m^2/K]	From 2700 (hot end) to 2350 (cold end)
Tube side convective HTC [W/m^2/K]	From 3350 (hot end) to 3200 (cold end)
Overall HTC [W/m^2/K]	From 910 (hot end) to 830 (cold end)
Average overall HTC [W/m^2/K]	869

to catch the effect of the working fluid pressure drops on the condenser design, showing that, at constant air face velocity, larger condensers with lower pressure drops on the working fluid side requires a higher fan consumption. Also the working fluid pressure drop is potentially an object for a wider optimization, but it is considered out of the scope of this work, and it will be considered for future publications.

The heatmaps in Fig. 13 depict the temperature distribution on both air and working fluid sides of the air-cooled condenser at design conditions, along each finite volume of the 7 passes tube depicted in Fig. 6.

In addition to the sizing of the heat exchanger, the air side pressure drops, evaluated according to the Marković correlation [56], are shown for a wide range of air face velocity and different ambient temperatures in Fig. 14, computed according to this specific configuration of a bank of staggered tubes proposed in Appendix E. The air side pressure drop model has been also compared with the Robinson and Biggs model [57], tailored to the fin geometry, showing deviations lower than 5 % across all range of interest of air face velocity. The results show an air side pressure drop dependency on the air velocity according to a power law with exponent 1.7, a conclusion coherent with the literature.

5. Cycle off-design: Results of the power block analysis

5.1. Results at given cycle minimum temperature and variable thermal input

This section presents the effect of variable thermal input and minimum temperature on the off-design performance of the cycle. The results of the off-design simulations are reported in Fig. 15, not considering the coupling between the cycle and the ambient conditions. The results are
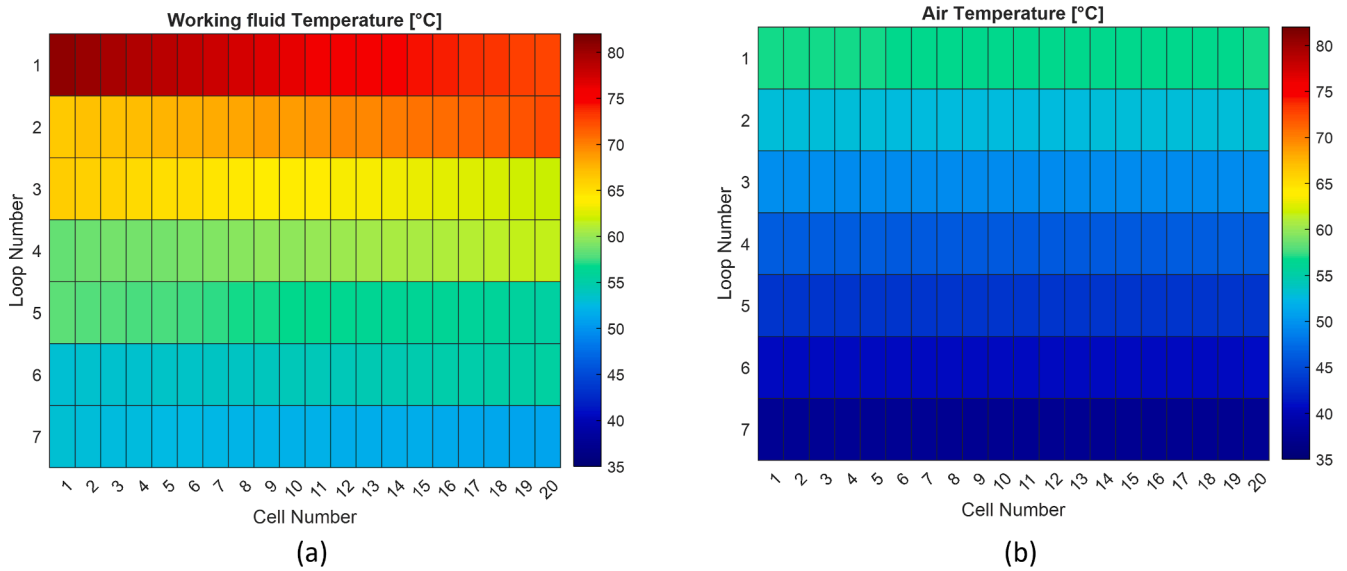
Fig. 13. Temperature distribution across the tube of the air condenser: working fluid side (a), air side (b).
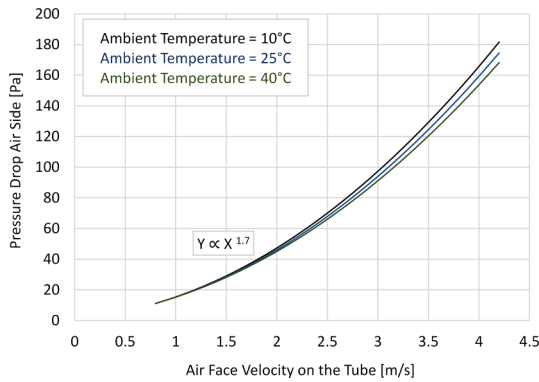

Fig. 14. Dependency on the air-side pressure drop on the air face velocity over the finned tube represented in Fig. 6 and characterized in Appendix E.

initially presented as function of the cycle minimum temperature and the thermal input, as detailed in Fig. 4, considering a thermal input ranging from the 100 % down to 40 % of the nominal value.

Results point out almost linear trends of the mass flow rate, pressures and temperatures involved, with an inversion of some trends only where the limit of cold end pinch point at the PHE is met (i.e. where the working fluid temperature at PHE inlet is higher than 416 °C, as described in Table 6) and the HTF temperature at PHE outlet increases. In these conditions, as the cold end temperature difference is fixed at 4 °C and cannot be furtherly reduced, the only solution to control the mean logarithmic temperature difference across the PHE is to increase the TIT. The simulations at cycle minimum temperature of 31 °C, instead, are not presented below 50 % of the design thermal input because the minimum value of maximum pressure is met. From the description of the turbine pressure ratio, the lower the cycle minimum temperature, the higher the pressure ratio: this aspect would imply a higher reduced mass flow rate at the turbine inlet and therefore a higher isentropic efficiency of the turbine, according to the turbine map in Fig. 8. This result outlines the importance of designing transcritical

cycles at the highest cycle minimum pressure.

Analyzing the nominal minimum temperature case (51 °C), it is possible to notice that the cycle efficiency reduction with the decrease of thermal input is initially contained, with respect to the design value, at around 0.7 percentage points at 70 % thermal input. This is possible thanks to the increased effectiveness of the recuperator, since its heat transfer area results oversized as the working fluid mass flow rate reduces (Fig. 15, top right). The enhanced internal heat recovery increases the working fluid temperature at the PHE inlet (Fig. 15, top center) with a positive effect on the cycle thermodynamic efficiency. As the load is further reduced, the reduction of the cycle pressure ratio (Fig. 15, bottom center) counterbalance more and more this effect, eventually causing a marked decrease in the gross cycle efficiency, also due to the much lower turbine and pump isentropic efficiency.

As the calculation of the PHE HTC in off-design conditions is a computationally expensive process, Appendix G details a possible approach to model it without solving the HX for each finite-volume: the approach in the appendix can be adopted in future analysis in case simplified models for the HX will be of interest.

5.2. Results at variable ambient temperature and thermal input

5.2.1. Condenser fan speed at design conditions

In this chapter, the coupling between the power cycle in off-design conditions and the air-cooled condenser is analyzed. The off-design model of the condenser computes, for each cycle off-design condition, the air face velocity (i.e. the volumetric flow rate of the air) needed to solve the heat transfer problem given an ambient temperature, as shown in Fig. D1. The results are presented in Fig. 16 for the range of cycle thermal inputs and cycle minimum temperatures of Fig. 15.

Fig. 16 on the right shows the control strategy chosen to regulate the air-cooled condenser and its effect on the off-design behavior of the plant at a thermal load equal to 80 % of the design value. The air-cooled condenser is not controlled (fixed fan velocity) in an ambient temperature range from 18 °C to 39 °C, and thus the power cycle minimum temperature varies in a range between 31 °C and 51 °C, respectively. When the ambient temperature is higher than 39 °C, it is not possible
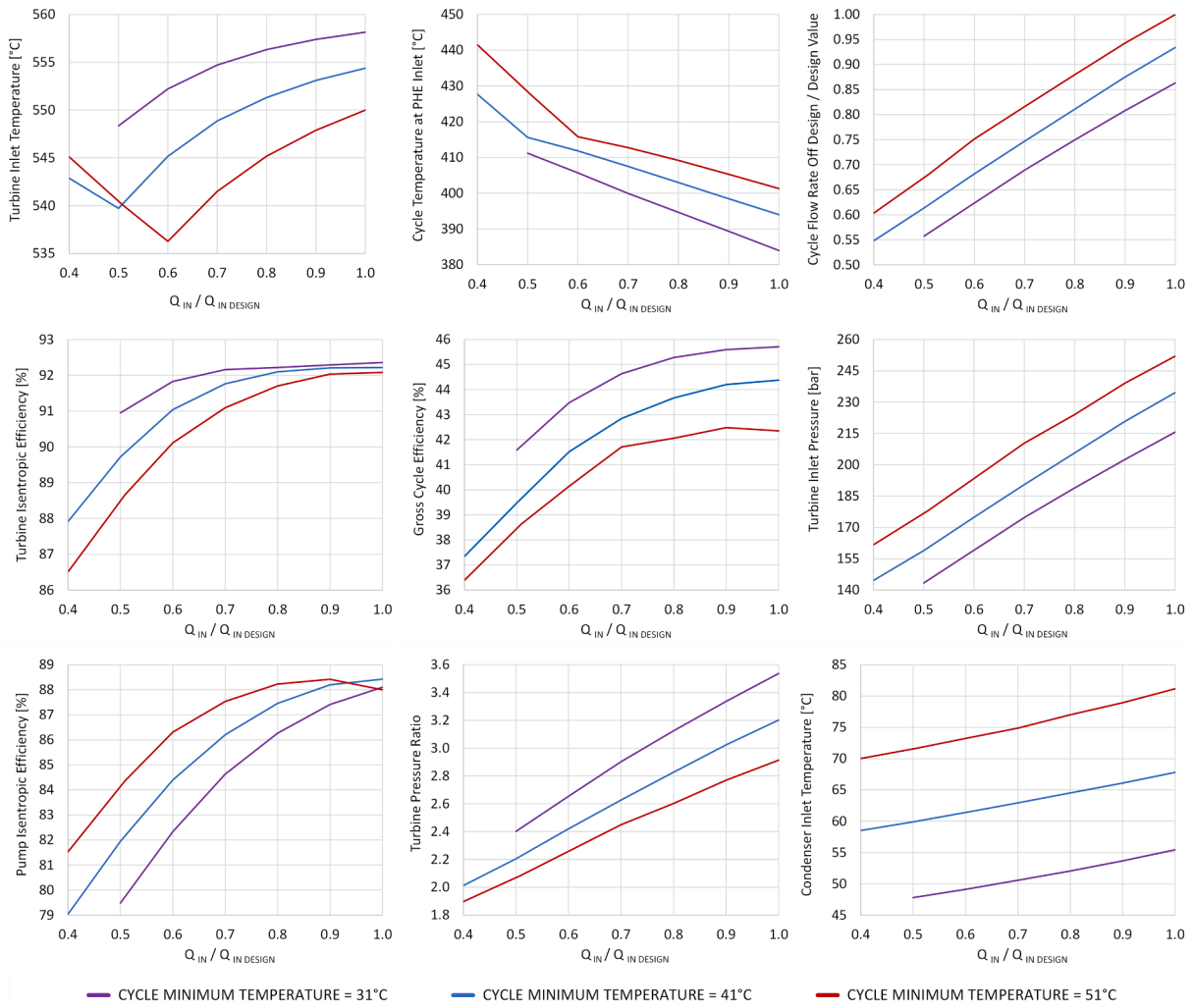
Fig. 15. Off-design results of the power cycle at given cycle minimum temperature and variable thermal input.
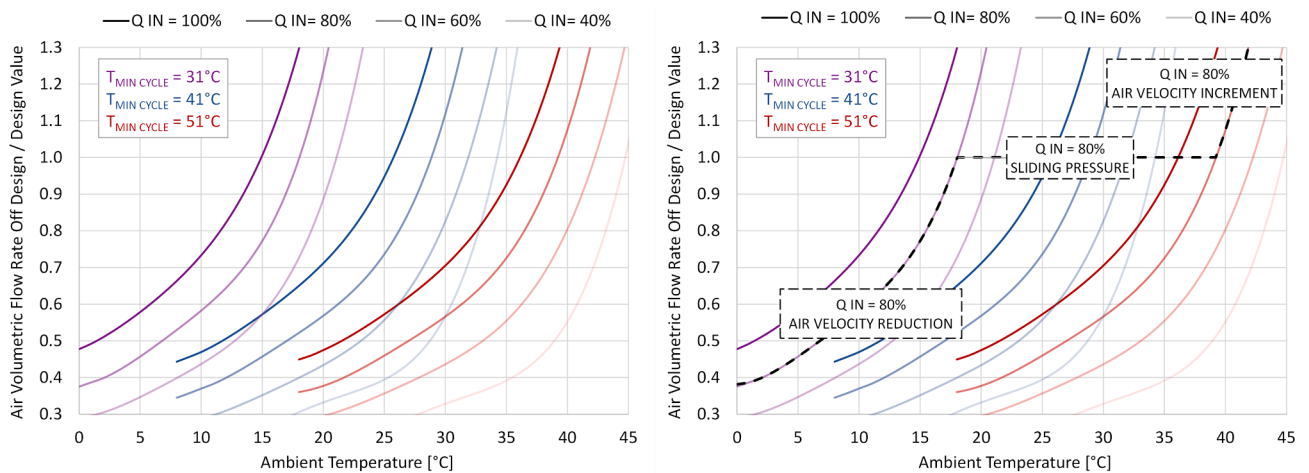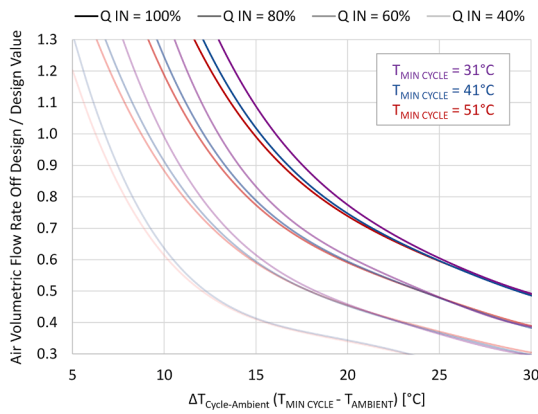

Fig. 16. Volumetric flow rate delivered by the fan as function of the ambient temperature, the thermal input and the cycle minimum temperature in off-design conditions.

Fig. 17. Volumetric flow rate of air as function of the temperature difference between the cycle minimum temperature and the ambient, for various off-design conditions.

anymore to achieve a cycle minimum temperature lower or equal to 51 °C with the nominal volumetric flow rate of the cooling air, thus the fan rotational speed should increase. The rotational speed limit of 130 % of the design value is reached at an ambient temperature around 42 °C with the cycle in this condition: above this ambient temperature it is no longer possible to run the plant at 80 % of the thermal load. On the other hand, for ambient temperatures below 18 °C the fan speed is reduced in order to avoid decreasing the cycle minimum temperature below 31 °C. This solution is feasible down to 30 % of the nominal value of the fan rotational speed, corresponding to an ambient temperature below 0 °C, maintaining a cycle minimum temperature of 31 °C. Below this rotational speed value the only possibility to run the plant at 80 % of the thermal load relies in shutting down some of the fans of the air cooled condenser and cooling some tube banks just by means of natural convection with the ambient air. This solution has not been explored in this work as the uneven cooling of the tube banks could lead to an unbalanced flow distribution and issues related to the working fluid composition at the condenser outlet. Ultimately, to overcome the limitations of the upper and lower limits in ambient temperature dictated by the rotational speed operational range of the condenser, it is always possible to modify the thermal input to the cycle.

The solutions of the air-cooled condenser in off-design are also reproposed in Fig. 17 to show the dependency of the volumetric air flow rate on the temperature difference between the ambient and the cycle minimum temperature ($\Delta T_{Cycle-Ambient} = T_{Min\,Cycle} - T_{ambient}$). Considering only conditions at design air volumetric flow rate, with the power cycle is operated in sliding pressure, the correlation in Equation (2) is satisfied:

$$\Delta T_{Cycle-Ambient} = \Delta T_{Cycle-Ambient,Design} \cdot \frac{\dot{Q}_{rejected}}{\dot{Q}_{rejected,Design}} \quad \left(for\, \dot{V}_{air} = \dot{V}_{air,Design} \right) \quad (2)$$

This simple but effective approach can help in determining the actual coupling between the off-design conditions of the cycle and the ambient temperature presented in Fig. 4, which is one of the main scopes of the cycle off-design analysis. Accordingly, the approach proposed in this work for the control of the air-condenser fans is to operate them at constant speed in design conditions, when possible, modifying the power cycle conditions according to its control in sliding pressure.

Thanks to this approach, coupling each solution of the power cycle in off-design to an ambient temperature, it is possible to move from a

representation of the results as shown in Fig. 15 to the results of Fig. 18, where both the cycle minimum temperature and the ambient temperature (dotted lines) are introduced.

Considering these results, it is possible to run the cycle in sliding pressure from ambient temperatures of 36 °C to 24 °C for any thermal input: at ambient temperatures of 40 °C and higher, full load solutions can be achieved only at the maximum cycle minimum temperature (of 51 °C) by increasing the fan speed of the air condenser. At the same time, for ambient temperatures below 20 °C it is possible to run the cycle only at the minimum value of cycle minimum temperature (31 °C) and decreasing the velocity of the condenser fans.

Most of the trends of Fig. 18 are linear in terms both of ambient temperature and cycle thermal input, as the working fluid temperature at PHE inlet, the cycle maximum pressure and turbine pressure ratio, the working fluid mass flow rate, both the turbine and pump efficiencies. The cycle efficiency, instead, shows larger gradients with respect to the ambient temperature at high thermal load, and the turbine inlet temperature is characterized by an inversion of trend for conditions of off-design of the HTF at the PHE outlet, according to the limits of Table 6. The net electric power block efficiency (computed from the gross cycle efficiency, adding the electromechanical losses and the auxiliary consumption of the air condenser) presents a strong variability in off-design, moving from a maximum value of 44.5 % at low ambient temperatures and high load, down to 37 % at low load and more adverse ambient conditions.

5.2.2. Condenser fan speed off-design conditions

When the ambient temperature is lower than 20 °C or slightly higher than the design value it is possible to modify the rotational speed of the condenser fan to reject the necessary heat into the environment at fixed cycle conditions, as shown in Fig. 16. Under this assumption, the resulting net electric power block efficiency is computed from the one of the cycle (including the electromechanical losses of the turbomachinery) and considering the variable fan consumption, computed according to the air-side pressure drop of presented in Fig. 14. The resulting trend of the net power block cycle efficiency is depicted in Fig. 19, as a contour plot with both the thermal input and the ambient temperature as independent variables.

By changing the rotational speed of the condenser fans the range of admissible ambient temperatures expands down to 0 °C at full load, and 8 °C at 50 % thermal load. On the other hand, much smaller variations of the maximum admissible ambient temperature are computed, of around 3 °C, by increasing the fan speed to the maximum value.

The results show a strong and very positive dependency of the cycle efficiency on the ambient temperature, suggesting setting the power cycle design conditions at both a high ambient temperature and a high cycle minimum temperature: the performance at design conditions, in fact, can be reached at a 55 % load with an ambient temperature of 20 °C, which is only 16 °C lower than the value at design conditions.

6. Conclusions

This work presented the methodology suggested for a detailed analysis of the performance in off-design conditions of a transcritical simple recuperative cycle working with CO_2-based mixtures as working fluid. The mixture adopted, $CO_2 + C_6F_6$, was identified in previous works within the H2020 SCARABEUS project as very promising from a techno-economic point of view for state-of-the-art CSP plants, adopting solar salts as heat source for the power cycle. Moreover, its thermodynamic and transport properties are computed with dedicated models, fitted on experimental data of the fluids: the need of specific models
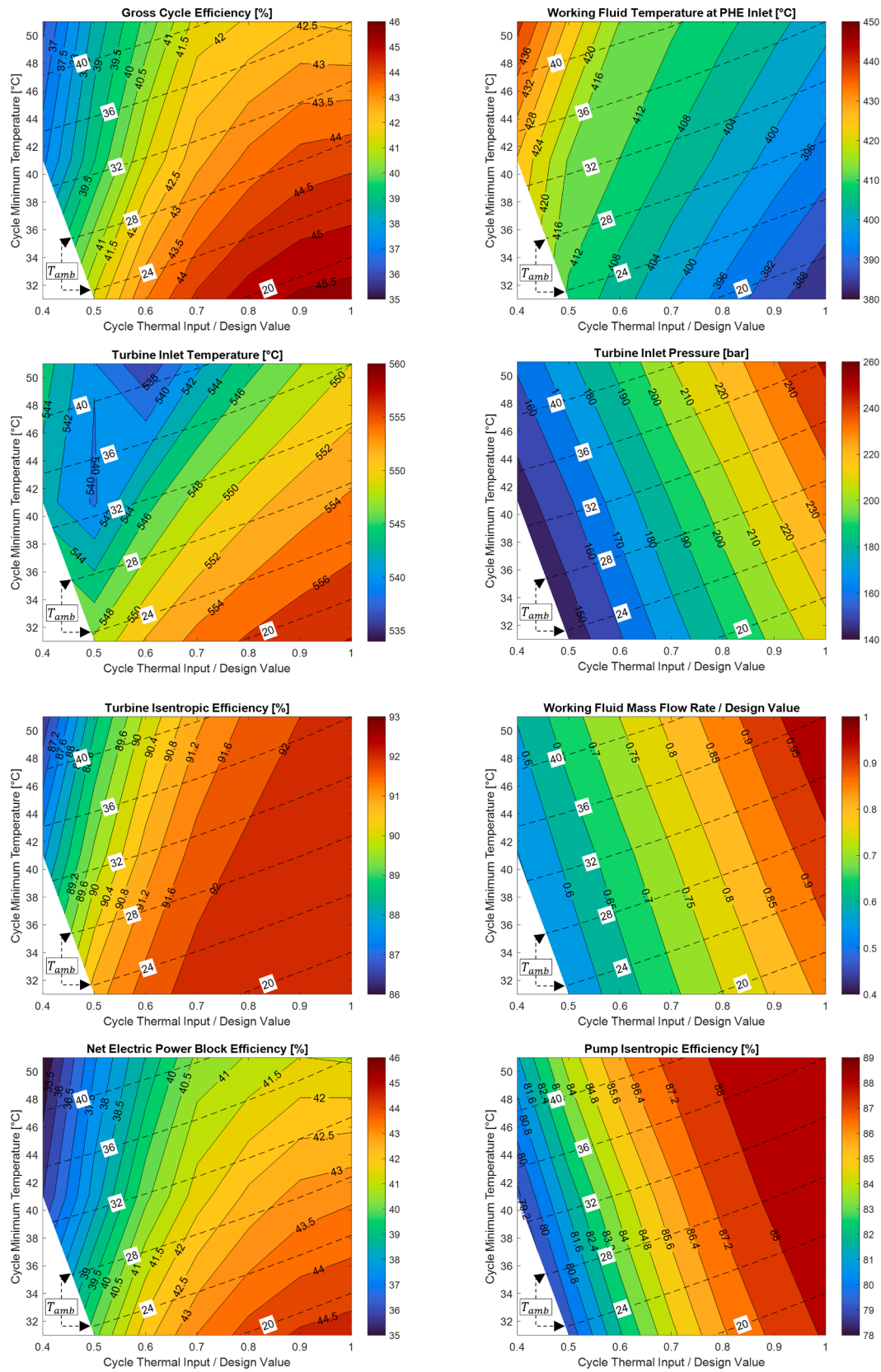
Fig. 18. Off-design resulting parameters of the power cycle investigated operating in sliding pressure, at constant fan speed of the air cooled condenser.
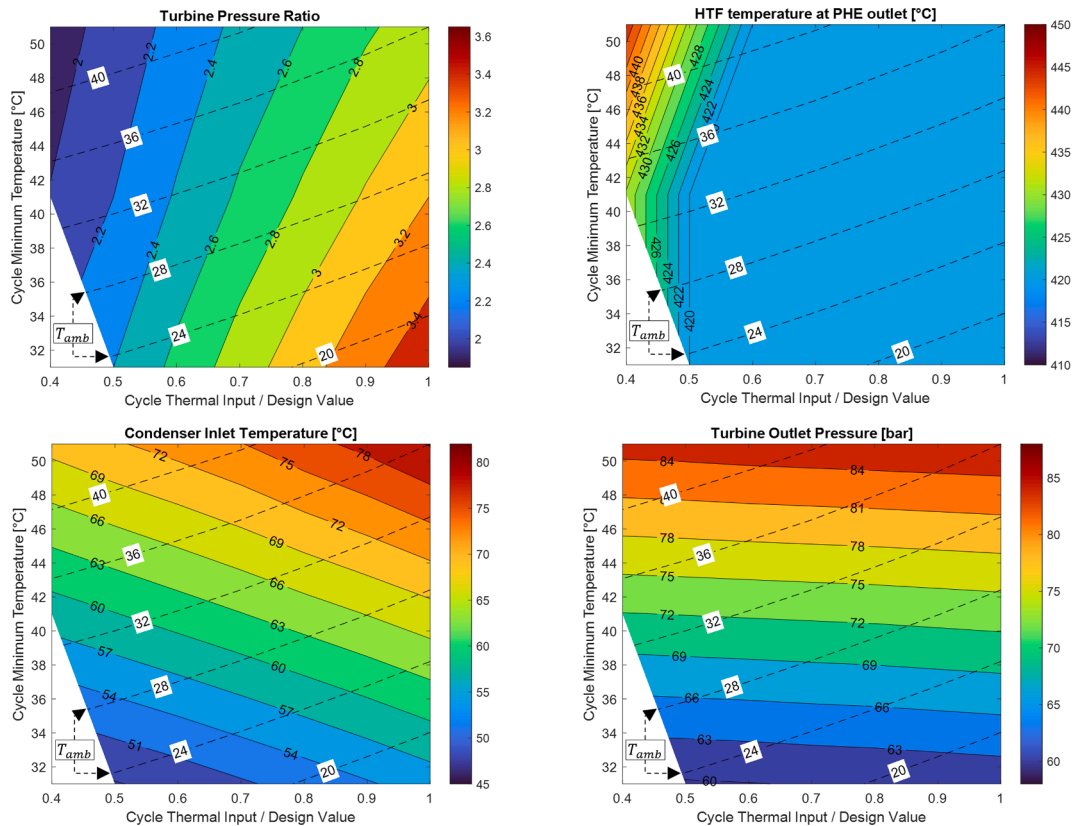
Fig. 18. (*continued*).

based on the mixture characteristics marks a significant difference with the same simulations based on supercritical CO_2 cycles.

The cycle analysis included detailed 1-D MATLAB models for the design of all the heat exchangers, and a detailed design of the turbine, allowing for a direct solution of the off-design performance of each cycle component under any circumstances and boundary conditions. The cycle simulations were carried out in off-design conditions by varying both the thermal input to the power cycle and the ambient temperature. Solutions at constant rotational speed of the air-condenser fan are considered to deliver the highest efficiency, keeping the power cycle in sliding pressure. The calculations are carried out solving each cycle component up to convergency on the overall characteristics of the cycle (temperature, pressure and mass flow rate in all conditions): this may represent a limit of this work due to the high computational resources employed.

The results indicated that the high net electric cycle efficiency computed in nominal conditions are still possible down to 80 % of the thermal input (between 42 % and 45 %, depending on the ambient temperature), while good efficiencies can be still reached down to 50 %-60 % of the thermal input, corresponding to around 45–55 % of the electric output. This proves the suitability of the CSP plant to efficiently follow a residual load curve during part load operation. Moreover, reducing to the minimum the fan speed of the condenser can allow for operation with ambient temperatures 20 to 25 °C lower than the value computed at nominal fan rotational speed, extending the ambient temperature range to any season, considering a good location for CSP. On the other hand, running the condenser at its maximum speed resulted in a small gain in allowable ambient temperature. Accordingly, the choice of selecting a high cycle minimum temperature and a high ambient

temperature at design conditions has been effectively proven and confirmed as a good design practice.

Comparing the net electric cycle performances with simulations of steam cycles from literature for the same application, it is clearly noticeable an increment of around 3.5 % to 4 % in absolute terms (i.e. 9 % in relative terms) of the net electric cycle efficiency at full load, for any ambient temperature, and 2.5 % to 3 % (about 7 % in relative terms) at 60 % thermal input. The positive results proved the good performances of simple recuperative transcritical power cycles working with CO_2-mixtures, both from a design point of view and especially from an off-design perspective.

To expand the content of this work, future studies can replicate the analysis on different working fluids (mixtures and dopant compositions) and plant layouts, to evidence the dependency of the cycle efficiency variation in off-design on these parameters. The cycle performances presented in this work can be then compared with the ones of a more conventional steam and sCO2 cycles, assuming the same boundary conditions and methodology. Additionally, a techno-economic analysis with the goal to compute net present values and internal rate of return can be carried out to account for the impact of the variable cycle efficiency along the year, including the variable ambient temperature and the load requested from the grid, including capital cost function from literature for the solar plants and the power block. Finally, as the off-design conditions are computed in this work, a further work could be performed by including information about the system thermal inertia to model the transients of the power block, to properly define ramp up and shut down curves useful in the simulations when the power block responds to the demand curve.
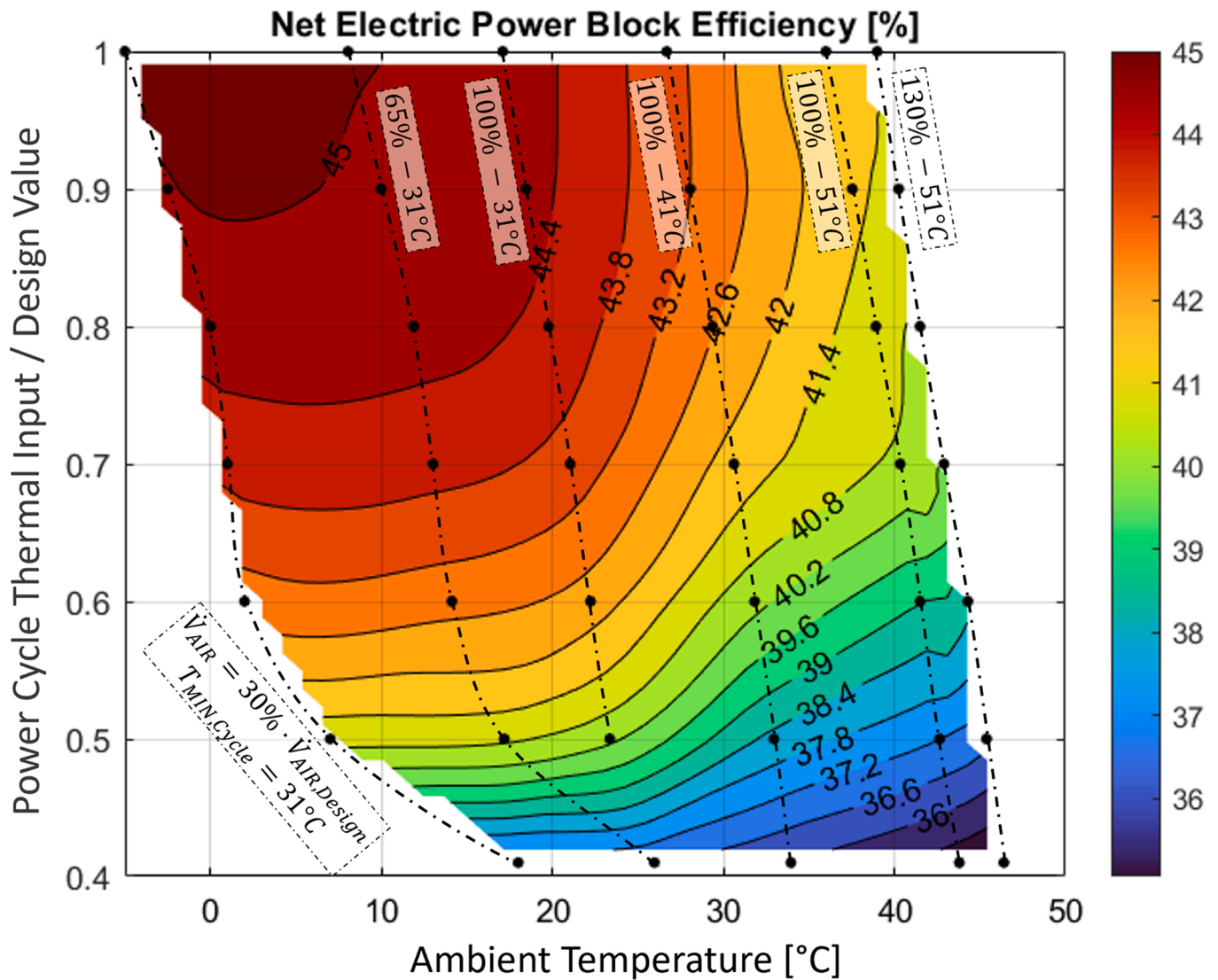
Fig. 19. Net electric power block efficiency of the power cycle in off-design as function of the ambient conditions and the thermal input.

Declaration of Competing Interest

The authors declare that they have no known competing financial interests or personal relationships that could have appeared to influence the work reported in this paper.

Data availability

Data will be made available on request.

Acknowledgements

Appendix A. Flowcharts of the design and Off-Design MATLAB model for the recuperator
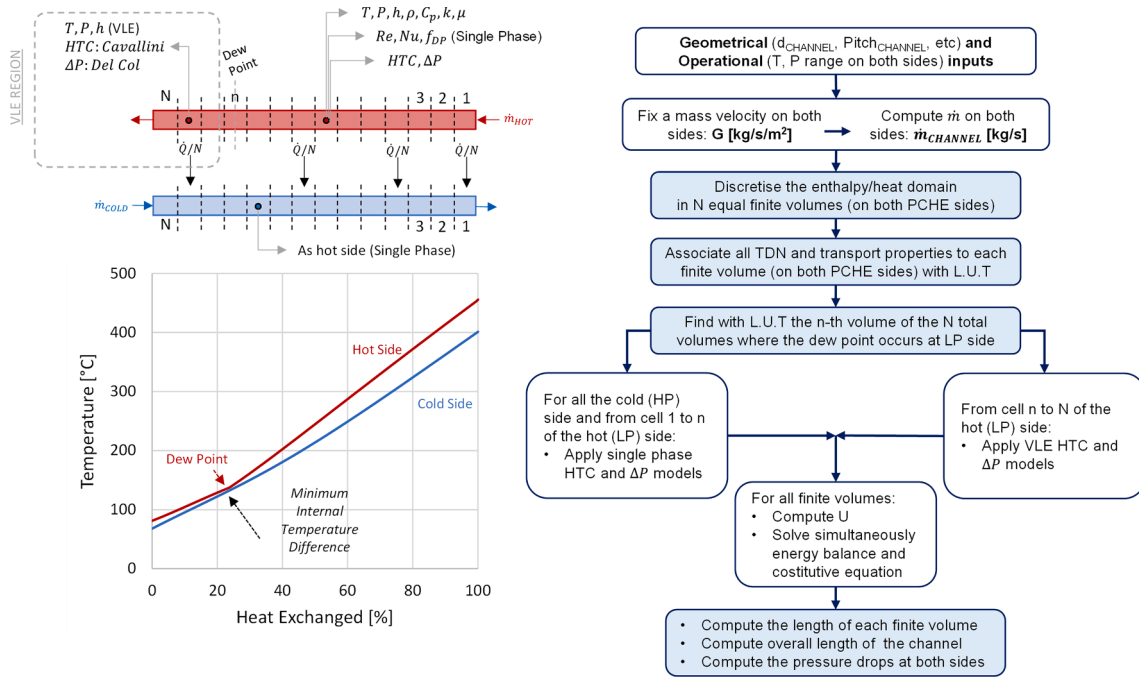
See Fig. A1, Fig. A2

Fig. A1. Methodology for the design of a PCHE recuperator with a part of the low-pressure side occurring in VLE conditions.
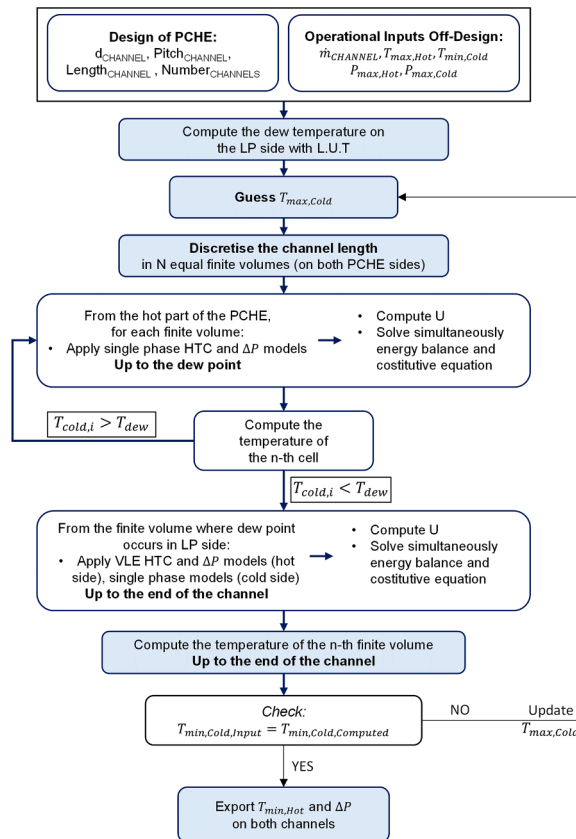

Fig. A2. Methodology for the off-design model of the PCHE recuperator with a part of the low-pressure side occurring in VLE conditions.

Appendix B. Validation of the MATLAB code for S&T HX with THERMOFLEX results

The results of this appendix refer to the comparison between the design tool adopted in MATLAB of this work for the design of S&T HX, detailed in Fig. 5, and the results of THERMOFLEX v29, for validation purposes.

The comparison has been carried out varying the baffle number in the MATLAB model, minimizing the deviation in overall heat transfer area between the two models. The calculations have been carried out on pure CO_2 as working fluid, for sake of simplicity, but the validity of the MATLAB model can be extended to any working fluid. The comparison proposes both the cases with S&T adopted as PHE for CSP applications with solar salts as HTF (Case 1 and 2) and for a case of S&T used as gas cooler of the power cycle, with water as cooling medium (Case 3). The comparison offers optimal deviations (in the range around 2 %) between the main geometrical results of two models for cases for PHE. Moreover, it still presents good results for the case study where the S&T is used as gas cooler (Table B1 and Table B2).

Table B1
Design parameters of the PHE designed to validate the Matlab model with THERMOFLEX results.

	Case 1	Case 2	Case 3
HTF (shell)/Working fluid (tube)	Solar Salts/CO2	Solar Salts/CO2	Water/CO2
CO2 pressure [bar]	254	254	100
Temperature range HTF [°C]	575–400	575–400	80–20
Temperature range working fluid [°C]	550–380	500–350	100–50
Mass flow rate working fluid/HTF [kg/s]	1000/795.6	100/70.24	100/47.82
Tube material	Inconel 617	Inconel 617	Carbon Steel
Tube outer diameter/Thickness [mm]	20/3	18/3	20/3
Shell diameter-to-Baffle spacing ratio	0.5	0.5	0.5
Tube-to-Pitch ratio/Tube layout	1.6/Rotated square	1.6/Rotated square	1.6/Rotated square
Thermal Power [MW$_{th}$]	212.6	18.8	12.0

Table B2
Comparison between the Matlab model and THERMOFLEX for the design of the S&T PHE.

	Case 1 (Matlab)	Case 1 (THERMOFLEX)	Deviation [%]
Tube external HX area [m^2]	11 501	11 370	1.2
Tube number	5 495	5 430	1.2
Tube length [m]	33.31	33.33	0.1
Shell diameter [m]	2.70	2.78	3.0
Baffle number	23	24	4.2
Tube side pressure drop [bar]	1.49	1.25	16.1
Average tube side HTF [W/m^2/K]	2 676	2 946	9.2
Overall HTC [W/m^2/K]	834	825	1.1
	Case 2 (Matlab)	**Case 2 (THERMOFLEX)**	**Deviation [%]**
Tube external HX area [m^2]	368	372	1.1
Tube number	676	691	2.2
Tube length [m]	9.64	9.51	1.4
Shell diameter [m]	0.88	0.89	1.1
Baffle number	21	22	4.5
Tube side pressure drop [bar]	0.48	0.68	29.4
Average tube side HTF [W/m^2/K]	2 962	3 162	6.3
Overall HTC [W/m^2/K]	828	815	1.6
	Case 3 (Matlab)	**Case 3 (THERMOFLEX)**	**Deviation [%]**
Tube external HX area [m2]	791	856	7.6
Tube number	1 551	1 480	4.8
Tube length [m]	8.11	9.21	11.9
Shell diameter [m]	1.47	1.43	2.8
Baffle number	10	12	16.7
Tube side pressure drop [bar]	0.01	0.06	83.3
Average tube side HTF [W/m^2/K]	1 581	1 415	11.7
Overall HTC [W/m^2/K]	602	568	6.0

Appendix C. Condenser design for different working fluid pressure drop

See Table C1)

Table C1
Effect of the working fluid pressure drop in the condenser on the condenser design.

	Larger Condenser	Design condition	Smaller Condenser
Working fluid pressure drop [bar]	0.5	1	2
Number of tubes	3'830	2'759	2'034
Pass length [m]	8.2	10.7	14.0
External condenser area (air side) [m^2]	392'029	370'924	354'256
Overall HTC [W/m^2/K]	22.9	24.9	26.6
Air Temperature difference [°C]	22.1	23.0	23.9
Electric Fan Consumption [MW$_{el}$]	0.89	0.80	0.72

Appendix D. Flowcharts of Off-Design sub-codes of PHE-turbine and the condenser
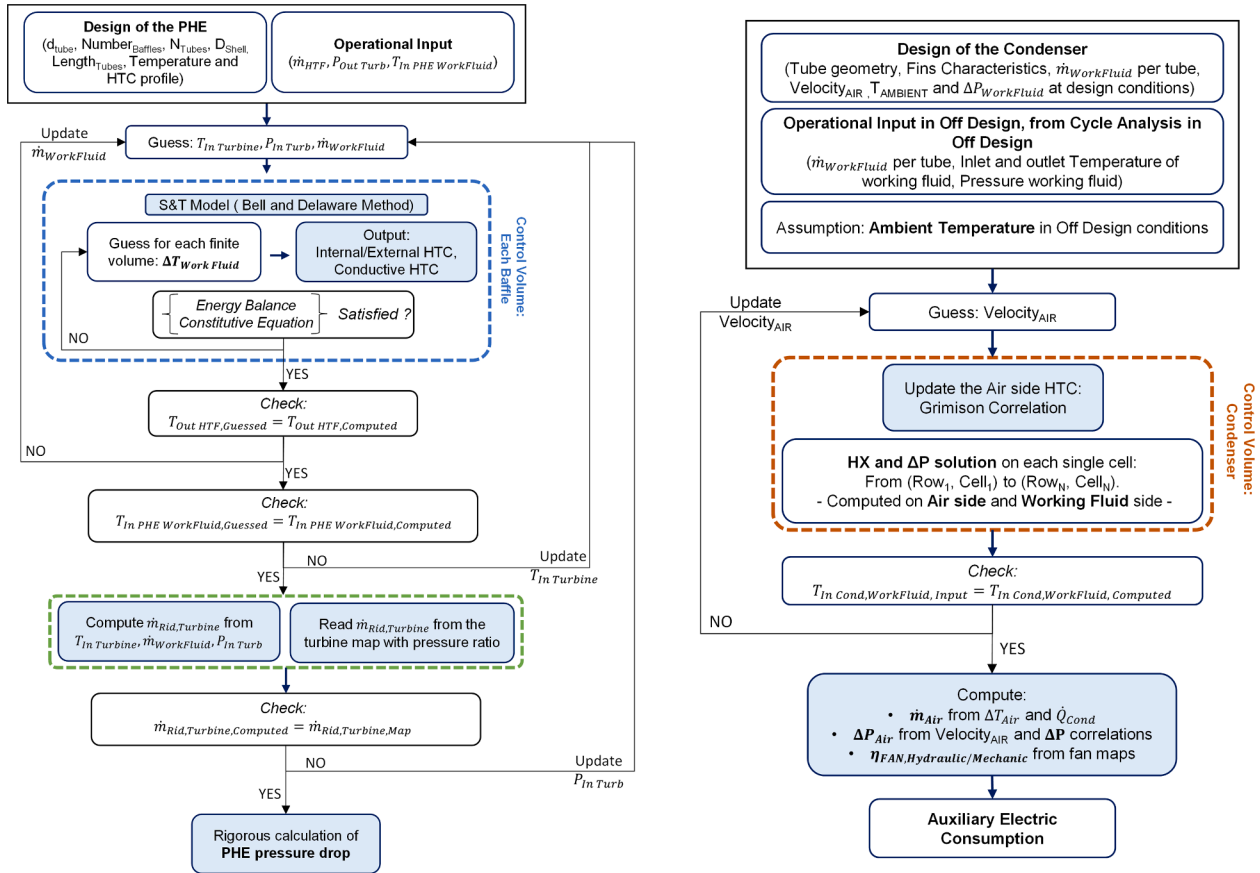
See Fig. D1

Fig. D1. Methodology for the off-design simulations of the PHE and the condenser.

Appendix E. Details on the geometry of the recuperator, PHE and condenser

See Table E1, Table E2, Table E3

Table E1
Characteristics of the various channels of the PCHE.

Characteristic of the PCHE	Value
Channel diameter [mm]	2
Plate thickness [mm]	0.5
Pitch between channels [mm]	2.4
Internal surface roughness [mm]	0.01
Material	Stainless Steel 316
Material thermal conductivity [W/m/K]	15

Table E2
Characteristics of the S&T PHE adopted for the cycle.

Characteristic of the S&T PHE	Value
Tube arrangement angle [°]	45
Tube external characteristics	Flat, Unfinned
Tube pitch/Tube outer diameter ratio	1.5
Baffle spacing/Shell diameter ratio	0.5
Baffle cut/Shell diameter ratio	0.3
Tube internal roughness [mm]	0.01
Tube material	Inconel 617
Material thermal conductivity [W/m/K]	$0.0185 \bullet T\,(°C) + 10.25$
Tube internal diameter [mm]	17
Tube thickness [mm]	3.5

Table E3
Characteristics of the finned-tube air-cooled condenser.

Characteristic of the condenser	Value
Tube internal/external diameter [mm]	20.76/26.8
Number of pass/number of rows per tube	7/7
Tube disposition	Staggered
Longitudinal/transversal tube pitch [mm]	57.7/66.7
Fin type	Circular and flat
Fin spacing/height [mm]	2.52/15.9
Fin thickness [mm]	0.3
Fin efficiency [%]	77.5
Area ratio (air side/working fluid side)	27.3
Tube material	Carbon steel
Fin material	Aluminum 1100-annealed

Appendix F. Details on the mesh used in the turbine analysis in CFD

A mesh independence study has been conducted to evaluate the validity at off-design conditions of the mesh size selected at the design point, presented in the author's previous publication [58]. To do so, a 4-stage 130 MW turbine operating with the $CO_2 + C_6F_6$ mixture was investigated, taken as a reference case: this reference case is adopted to simplify the analysis, assuming that the same flow physics of this reference case applies also to the 9 stages turbine presented in Fig. 9 (specifically the flow separation phenomenon). The relationship between the average number of grid points per stage and the total-to-total efficiency is presented in Fig. F1 for the design condition and a point operating at 50 % of the design mass flow rate. Convergence of efficiency at off-design required around 2.8 million grid points per stage compared to 0.6 million grid points at the design point, maintaining a 0.2 % efficiency tolerance. Therefore, a 2.8 million grid points are adopted for the simulations of Fig. 8.
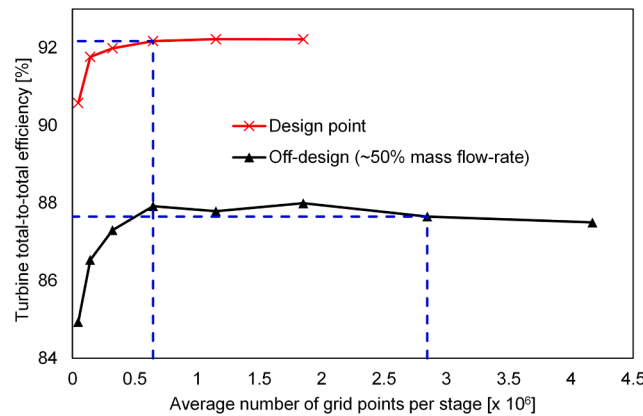
Fig. F1. Grid convergency analysis on the turbine efficiency developed for a reference case in CFD (a 4-stage 130 MW turbine operating with the same working fluid of this work).

## Appendix G. Simplified modeling of the PHE off-design

An additional information is collected from the simulations presented in Fig. 15, which can help identifying a simplified and quicker solution to the overall off-design simulations of the power cycle. As the PHE off-design is built as a complex and computationally expensive code (according to the Bell and Delaware model), its results are more carefully catalogued and analyzed to scrutinize the possibility of foreseeing a correlation to compute the overall HTC of the HX without run the whole model for each finite-volume. This correlation can have the form expressed in Equation (3), neglecting the dependency on the HTF pressure, since it is modelled as an ideal liquid according to literature [59]:

$$U_{PHE} = f\left(PHE_{design}, \ \dot{m}_{HTF}, \ Temperature_{HTF}, \ \dot{m}_{WorkingFluid}, \ Pressure_{WorkingFluid}, \ Temperature_{WorkingFluid} \right) \tag{3}$$

Analyzing the case-specific S&T PHE of this work for CSP applications with a CO_2-based working fluid, with solar salts on the HTF side, it is possible to conclude that the HTF temperature range is nearly constant in off-design conditions, along with the temperature range of the working fluid, both not presenting drastic variations. Under these assumptions, the overall HTC is proposed in dimensionless terms as in Equation (4):

$$U_{PHE, \ Off-Design} \Big/ U_{PHE, \ Design} = f\left(\dot{m}_{HTF}, \ \dot{m}_{WorkingFluid}, \ Pressure_{WorkingFluid} \right) \tag{4}$$

The simulations carried out in this work are then organized in a single correlation, proposed as a polynomial function of the product between the HTF mass flow rate and the working fluid mass flow rate ($\dot{m}_{HTF} \cdot \dot{m}_{WorkingFluid}$), neglecting the dependency on the pressure of the working fluid. The resulting correlation modeling Equation (4) is proposed in Fig. G2, built upon four additional sets of simulations (denominated Case A, B, C and D): they are run as stand-alone off-design simulations of the PHE, with no connection to any other part of the power cycle, to simulate more generalized conditions.
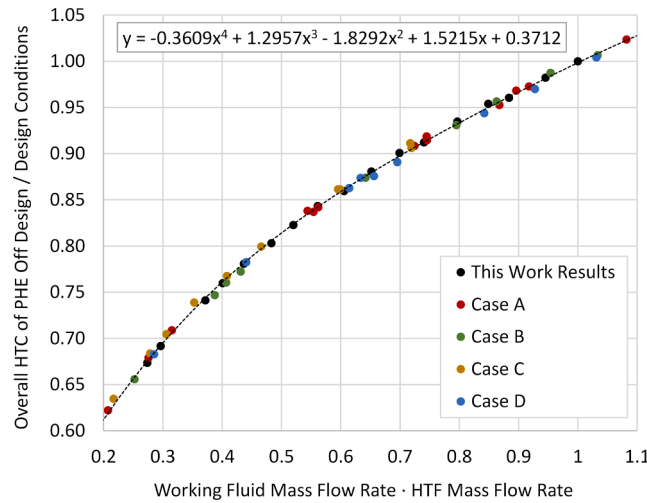
Fig. G2. Resulting overall HTC of the PHE computed by the Matlab model of this work, for various operating conditions and design of PHE.

The other four sets of simulations in Fig. G2 are characterized by various design of the PHE and different HTF outlet temperature (as listed in Table G1), to widen the validity of the correlation. Case B is proposed for a different design of the PHE, in a condition with 4 bar of tube-side pressure drop and a heat exchange area lower than the one of the PHE in this work. On the other hand, Case C and D, instead, evaluates the PHE performance at different HTF outlet temperature, to understand the dependency of this variable. For the four sets of simulations of Table G1, which do not correspond to solutions of the overall off-design model of the cycle, the working fluid conditions are varied randomly in a range coherent with the simulations carried out in this work. In particular: the mass flow rate is varied randomly between 35 % and 105 % of the design value, the temperature at the outlet of the PHE is varied randomly between 560 °C and 530 °C, the pressure of the working fluid is varied randomly between 140 bar and 250 bar, the temperature at PHE inlet is varied randomly between 370 °C and 415 °C.

Table G1
Characteristics of the four additional sets of simulations for the off-design of the PHE.

	PHE Design	HTF Outlet Temperature
Case A	This Work Design	This Work Value
Case B	Pressure Drop $\times$ 2, Area $\times$ 0.88 w/r/t This Work	This Work Value
Case C	This Work Design	This Work Value + 15 °C
Case D	This Work Design	This Work Value – 15 °C

The correlation proposed in this work to compute the off-design value of the HTC of a S&T PHE for CSP applications has the form of Equation (5), fitted on the simulations of Fig. G2 with an R^2 of 0.9993. To adopt this correlation, some crucial aspects must be considered: solar salts is considered as HTF, the working fluid of the power cycle is a CO_2-based fluid, and the simulations are run for a high-temperature S&T adopting Inconel as tube material, suitable to CSP applications.

$$\frac{U_{PHEOff-Design}}{U_{PHEDesign}} = -0.3609 \cdot \left(\dot{m}_{HTF} \cdot \dot{m}_{WorkingFluid} \right)^4 + 1.2957 \cdot \left(\dot{m}_{HTF} \cdot \dot{m}_{WorkingFluid} \right)^3 - 1.8292 \cdot \left(\dot{m}_{HTF} \cdot \dot{m}_{WorkingFluid} \right)^2 + 1.5215 \cdot \left(\dot{m}_{HTF} \cdot \dot{m}_{WorkingFluid} \right) + 0.3712$$

(5)

References

[1] D. Belverato, E. Martelli, M. Binotti, L. Pilotti, A. Giaconia, Part-Load of Steam Rankine Cycles for Solar Salts-Based Concentrating Solar Power Plants, in: Proceedings of the ASME Turbo Expo, American Society of Mechanical Engineers Digital Collection, 2022. https://doi.org/10.1115/GT2022-79378.

[2] S. El Marazgioui, A. El Fadar, Impact of cooling tower technology on performance and cost-effectiveness of CSP plants, Energy Convers. Manag. 258 (2022) 115448, https://doi.org/10.1016/J.ENCONMAN.2022.115448.

[3] W.T. Hamilton, A.M. Newman, M.J. Wagner, R.J. Braun, Off-design performance of molten salt-driven Rankine cycles and its impact on the optimal dispatch of concentrating solar power systems, Energy Convers Manag. 220 (2020) 113025, https://doi.org/10.1016/J.ENCONMAN.2020.113025.

[4] M.J. Wagner, A.M. Newman, W.T. Hamilton, R.J. Braun, Optimized dispatch in a first-principles concentrating solar power production model, Appl. Energy 203 (2017) 959–971, https://doi.org/10.1016/J.APENERGY.2017.06.072.

[5] M.J. Wagner, W.T. Hamilton, A. Newman, J. Dent, C. Diep, R. Braun, Optimizing dispatch for a concentrated solar power tower, Sol. Energy 174 (2018) 1198–1211, https://doi.org/10.1016/J.SOLENER.2018.06.093.

[6] L. Pilotti, M. Colombari, A.F. Castelli, M. Binotti, A. Giaconia, E. Martelli, Simultaneous design and operational optimization of hybrid CSP-PV plants, Appl. Energy 331 (2023), https://doi.org/10.1016/J.APENERGY.2022.120369.

[7] F. Crespi, D. Sánchez, J.M. Rodríguez, G. Gavagnin, Fundamental Thermo-Economic Approach to Selecting sCO2 Power Cycles for CSP Applications, Energy Procedia 129 (2017) 963–970, https://doi.org/10.1016/J.EGYPRO.2017.09.215.

[8] A. Lock, V. Bone, Off-design operation of the dry-cooled supercritical CO2 power cycle, Energy Convers. Manag. 251 (2022), 114903, https://doi.org/10.1016/J.ENCONMAN.2021.114903.

[9] M.T. White, G. Bianchi, L. Chai, S.A. Tassou, A.I. Sayma, Review of supercritical CO2 technologies and systems for power generation, Appl. Therm. Eng. 185 (2021), https://doi.org/10.1016/j.applthermaleng.2020.116447.

[10] M. Marchionni, M. Usman, L. Chai, S.A. Tassou, Inventory control assessment for small scale sCO2 heat to power conversion systems, Energy 267 (2023), https://doi.org/10.1016/J.ENERGY.2022.126537.

[11] A. Moisseytsev, J.J. Sienicki, Recent developments in s-CO2 cycle dynamic modeling and analysis at ANL, in: The 4th International Symposium–Supercritical CO2 Power Cycles, Pittsburgh, Pennsylvania, 2014.

[12] J. Yang, Z. Yang, Y. Duan, Off-design performance of a supercritical CO2 Brayton cycle integrated with a solar power tower system, Energy 201 (2020), https://doi.org/10.1016/J.ENERGY.2020.117676.

[13] D. Alfani, M. Astolfi, M. Binotti, P. Silva, E. Macchi, Off-design performance of CSP plant based on supercritical CO2 cycles, AIP Conf. Proc. 2303 (2020), 130001, https://doi.org/10.1063/5.0029801.

[14] T. Neises, Steady-state off-design modeling of the supercritical carbon dioxide recompression cycle for concentrating solar power applications with two-tank sensible-heat storage, Sol. Energy 212 (2020) 19–33, https://doi.org/10.1016/J.SOLENER.2020.10.041.

[15] D. Alfani, M. Astolfi, M. Binotti, P. Silva, Effect of the ambient temperature on the performance of small size sCO2 based pulverized coal power plants, in: 4th European SCO2 Conference for Energy Systems: March 23-24, 2021, Online Conference, 2021: pp. 379–388. https://doi.org/10.17185/duepublico/73981.

[16] S. Khatoon, M.H. Kim, Potential improvement and comparative assessment of supercritical Brayton cycles for arid climate, Energy Convers. Manag. 200 (2019), 112082, https://doi.org/10.1016/j.enconman.2019.112082.

[17] G. Manzolini, M. Binotti, D. Bonalumi, C. Invernizzi, P. Iora, CO2 mixtures as innovative working fluid in power cycles applied to solar plants. Techno-Economic Assess, Sol. Energy 181 (2019) 530–544, https://doi.org/10.1016/j.solener.2019.01.015.

[18] Scarabeus H2020 Project, (n.d.). https://www.scarabeusproject.eu/.

[19] Desolination H2020 Project, (n.d.). https://desolination.eu/ (accessed October 25, 2022).

[20] E. Morosini, A. Ayub, G. di Marcoberardino, C.M. Invernizzi, P. Iora, G. Manzolini, Adoption of the CO2 + SO2 mixture as working fluid in transcritical cycles: A thermodynamic assessment with optimized equation of state, Energy Convers Manag. 255 (2022), https://doi.org/10.1016/J.ENCONMAN.2022.115263.

[21] F. Crespi, P. Rodríguez de Arriba, D. Sánchez, A. Muñoz, Preliminary investigation on the adoption of CO2-SO2 working mixtures in a transcritical Recompression cycle, Appl. Therm. Eng. 211 (2022), https://doi.org/10.1016/J.APPLTHERMALENG.2022.118384.

[22] F. Crespi, P. Rodríguez de Arriba, D. Sánchez, A. Ayub, G. Di Marcoberardino, C. M. Invernizzi, G.S. Martínez, P. Iora, D. Di Bona, M. Binotti, G. Manzolini, Thermal efficiency gains enabled by using CO2 mixtures in supercritical power cycles, Energy 238 (2022), https://doi.org/10.1016/J.ENERGY.2021.121899.

[23] O.A. Aqel, M.T. White, M.A. Khader, A.I. Sayma, Sensitivity of transcritical cycle and turbine design to dopant fraction in CO2-based working fluids, Appl. Therm. Eng. 190 (2021), 116796, https://doi.org/10.1016/J.APPLTHERMALENG.2021.116796.

[24] G. Di Marcoberardino, E. Morosini, D. Di Bona, P. Chiesa, C. Invernizzi, P. Iora, G. Manzolini, Experimental characterisation of CO2 + C6F6 mixture: Thermal stability and vapour liquid equilibrium test for its application in transcritical power cycle, Appl. Therm. Eng. 212 (2022), https://doi.org/10.1016/J.APPLTHERMALENG.2022.118520.

[25] G. Manzolini, M. Binotti, E. Morosini, D. Sanchez, F. Crespi, G. Di Marcoberdino, P. Iora, C. Invernizzi, Adoption of CO2 blended with C6F6 as working fluid in CSP plants, in: AIP Conf Proc, AIP Publishing, 2022, p. 090005, https://doi.org/10.1063/5.0086520.

[26] E. Morosini, E. Villa, G. Quadrio, M. Binotti, G. Manzolini, Solar tower CSP plants with transcritical cycles based on CO2 mixtures: A sensitivity on storage and power block layouts, Sol. Energy 262 (2023), https://doi.org/10.1016/J.SOLENER.2023.05.054.

[27] M. Doninelli, E. Morosini, G. Gentile, L. Putelli, G. di Marcoberardino, M. Binotti, G. Manzolini, Thermal desalination from rejected heat of power cycles working with CO2-based working fluids in CSP application: a focus on the MED technology, Sustainable Energy Technologies and Assessments. (2023). Accepted article, In press, https://doi.org/10.1016/j.seta.2023.103481.

[28] E. Morosini, M. Binotti, G. Di Marcoberardino, C. Invernizzi, P. Iora, G. Manzolini, Adoption of CO2 Mixtures as Working Fluid for CSP Cycles with Linear Collectors and Molten Salts as HTF. SolarPaces Conference 2021, American Institute of Physics Inc., 2023.

[29] E. Morosini, G. Gentile, M. Binotti, G. Manzolini, Techno-economic assessment of small-scale solar tower plants with modular billboard receivers and innovative power cycles, in: J Phys Conf Ser, IOP Publishing, 2022: p. 012109. https://doi.org/10.1088/1742-6596/2385/1/012109.

[30] L.L. Vant-Hull, Central tower concentrating solar power systems, in: Concentrating Solar Power Technology: Principles, Developments, and Applications, Woodhead Publishing, 2021, pp. 267–310, https://doi.org/10.1016/B978-0-12-819970-1.00019-0.

[31] D. Alfani, M. Binotti, E. Macchi, P. Silva, M. Astolfi, sCO2 power plants for waste heat recovery: design optimization and part-load operation strategies, Appl. Therm. Eng. 195 (2021), 117013, https://doi.org/10.1016/J.APPLTHERMALENG.2021.117013.

[32] P. Wu, Y. Ma, C. Gao, W. Liu, J. Shan, Y. Huang, J. Wang, D. Zhang, X. Ran, A review of research and development of supercritical carbon dioxide Brayton cycle technology in nuclear engineering applications, Nucl. Eng. Des. 368 (2020), https://doi.org/10.1016/J.NUCENGDES.2020.110767.

[33] AspenTech, Aspen Plus | Leading Process Simulation Software | AspenTech, (n.d.). https://www.aspentech.com/en/products/engineering/aspen-plus.

[34] J. Gross, G. Sadowski, Perturbed-chain SAFT: An equation of state based on a perturbation theory for chain molecules, Ind. Eng. Chem. Res. 40 (2001) 1244–1260, https://doi.org/10.1021/ie0003887.

[35] G. Di Marcoberardino, E. Morosini, G. Manzolini, Preliminary investigation of the influence of equations of state on the performance of CO2 + C6F6 as innovative

[36] N. Zheng, Z. Li, J. Fang, J. Wei, Supercritical CO2 mixture Brayton cycle with floating critical points for concentrating solar power application: Concept and thermodynamic analysis, Energy Convers. Manag. 284 (2023), https://doi.org/10.1016/J.ENCONMAN.2023.116989.

[37] V. Illyés, E. Morosini, M. Doninelli, P.L. David, X. Guerif, A. Werner, G. Di Marcoberardino, G. Manzolini, Design of an Air-Cooled Condenser for CO2-Based Mixtures: Model Development, Validation and Heat Exchange Gain with Internal Microfins, in: Proceedings of the ASME Turbo Expo, American Society of Mechanical Engineers Digital Collection, 2022. https://doi.org/10.1115/GT2022-82438.

[38] S.I. Salah, M.A. Khader, M.T. White, A.I. Sayma, ; M Ac Khader@city, M.A.K. Uk, M.A. White@city, (M T W Uk, A.A. Sayma@city, A.I.S. Uk, Mean-Line Design of a Supercritical CO2 Micro Axial Turbine, Appl. Sci., 2020, Vol. 10, Page 5069. 10 (2020) 5069. https://doi.org/10.3390/APP10155069.

[39] S.I. Salah, F. Crespi, M.T. White, A. Muñoz, A. Paggini, M. Ruggiero, D. Sánchez, A. I. Sayma, Axial turbine flow path design for concentrated solar power plants operating with CO2 blends, Appl. Therm. Eng. 230 (2023), 120612, https://doi.org/10.1016/J.APPLTHERMALENG.2023.120612.

[40] S.I. Salah, M.T. White, A.I. Sayma, A comparison of axial turbine loss models for air, sCO2 and ORC turbines across a range of scales, International Journal of Thermofluids. 15 (2022), https://doi.org/10.1016/J.IJFT.2022.100156.

[41] S.F. Smith, A Simple Correlation of Turbine Efficiency, J. Royal Aeronaut. Soc. 69 (1965) 467–470, https://doi.org/10.1017/S0001924000059108.

[42] S.C. Kacker, U. Okapuu, A Mean Line Prediction Method for Axial Flow Turbine Efficiency, J. Eng. Power 104 (1982) 111–119, https://doi.org/10.1115/1.3227240.

[43] A. Abdeldayem, S. Salah, O. Aqel, M. White, A. Sayma, Design of a 130 MW axial turbine operating with a supercritical carbon dioxide mixture for the SCARABEUS project, in: Proceedings of 15th European Conference on Turbomachinery Fluid Dynamics & Thermodynamics ETC15April 24-28 2023, 2023.

[44] R.H. Aungier, Turbine Aerodynamics: Axial-Flow and Radial-Flow Turbine Design and Analysis, ASME Press, 2006. https://doi.org/10.1115/1.802418.

[45] A.S. Abdeldayem, M.T. White, A. Paggini, M. Ruggiero, A.I. Sayma, Integrated Aerodynamic and Structural Blade Shape Optimization of Axial Turbines Operating With Supercritical Carbon Dioxide Blended With Dopants, J. Eng. Gas Turbine Power. 144 (2022), https://doi.org/10.1115/1.4055232/1145514.

[46] V. Dostal, M.J. Driscoll, P. Hejzlar, A Supercritical Carbon Dioxide Cycle for Next Generation Nuclear Reactors, Technical Report MIT-ANP-TR-100. (2004) 1–317. https://doi.org/MIT-ANP-TR-100.

[47] D. Alfani, M. Astolfi, M. Binotti, S. Campanari, F. Casella, P. Silva, Multi Objective Optimization of Flexible Supercritical CO2 Coal-Fired Power Plants, in: Proceedings of the ASME Turbo Expo, American Society of Mechanical Engineers Digital Collection, 2019. https://doi.org/10.1115/GT2019-91789.

[48] V. Gnielinski, New Equations for Heat and Mass Transfer in Turbulent Pipe and Channel Flow, Int. J. Chem. Eng. 16 (1976) 359–368.

[49] A. Cavallini, D. Del Col, L. Doretti, M. Matkovic, L. Rossetto, C. Zilio, G. Censi, Condensation in Horizontal Smooth Tubes: A New Heat Transfer Model for Heat Exchanger Design, Heat Transf. Eng. 27 (2006) 31–38, https://doi.org/10.1080/01457630600793970.

[50] D. Del Col, A. Bisetto, M. Bortolato, D. Torresin, L. Rossetto, Experiments and updated model for two phase frictional pressure drop inside minichannels, Int. J. Heat Mass Transf. 67 (2013) 326–337, https://doi.org/10.1016/J.IJHEATMASSTRANSFER.2013.07.093.

[51] S. Fettaka, J. Thibault, Y. Gupta, Design of shell-and-tube heat exchangers using multiobjective optimization, Int. J. Heat Mass Transf. 60 (2013) 343–354, https://doi.org/10.1016/J.IJHEATMASSTRANSFER.2012.12.047.

[52] S. Kakaç, H. Liu, A. Pramuanjaroenkij, Heat Exchangers: Selection, Rating, and Thermal Design, CRC Press (2020), https://doi.org/10.1201/9780429469862.

[53] N.T. Weiland, B.W. Lance, S.R. Pidaparti, SCO2 power cycle component cost correlations from DOE data spanning multiple scales and applications, in: Proceedings of the ASME Turbo Expo, Am. Soc. Mech. Eng. (ASME), 2019. https://doi.org/10.1115/GT2019-90493.

[54] D. Alfani, M. Astolfi, M. Binotti, P. Silva, Part-Load Strategy Definition and Preliminary Annual Simulation for Small Size sCO2-Based Pulverized Coal Power Plant, J. Eng. Gas Turbine Power. 143 (2021), https://doi.org/10.1115/1.4051003/1108261.

[55] E.D. Grimison, Correlation and Utilization of New Data on Flow Resistance and Heat Transfer for Cross Flow of Gases Over Tube Banks, J. Fluids Eng. 59 (1937) 583–594, https://doi.org/10.1115/1.4020557.

[56] S. Marković, B. Jaćimović, S. Genić, M. Mihailović, U. Milovančević, M. Otović, Air side pressure drop in plate finned tube heat exchangers, Int. J. Refrig. 99 (2019) 24–29, https://doi.org/10.1016/J.IJREFRIG.2018.11.038.

[57] K.K. Robinson, D.E. Briggs, Pressure drop of air flowing across triangular pitch banks of finned tubes, Chem. Eng. Prog. Symp. 62 (1966) 177–184.

[58] A.S. Abdeldayem, S.I. Salah, M.T. White, A.I. Sayma, A Modified Loss Breakdown Approach for Axial Turbines Operating With Blended Supercritical Carbon Dioxide, J. Eng. Gas Turbine Power. 145 (2023), https://doi.org/10.1115/1.4062478.

[59] G. Manzolini, G. Lucca, M. Binotti, G. Lozza, A two-step procedure for the selection of innovative high temperature heat transfer fluids in solar tower power plants, Renew. Energy 177 (2021) 807–822, https://doi.org/10.1016/J.RENENE.2021.05.153.